



Detailing cloud property feedbacks with a regime-based decomposition

Mark D. Zelinka¹ · Ivy Tan² · Lazaros Oreopoulos³ · George Tselioudis⁴

Received: 15 April 2022 / Accepted: 29 August 2022 / Published online: 11 September 2022
© The Author(s), under exclusive licence to Springer-Verlag GmbH Germany, part of Springer Nature 2022

Abstract

Diagnosing the root causes of cloud feedback in climate models and reasons for inter-model disagreement is a necessary first step in understanding their wide variation in climate sensitivities. Here we bring together two analysis techniques that illuminate complementary aspects of cloud feedback. The first quantifies feedbacks from changes in cloud amount, altitude, and optical depth, while the second separates feedbacks due to cloud property changes within specific cloud regimes from those due to regime occurrence frequency changes. We find that in the global mean, shortwave cloud feedback averaged across ten models comes solely from a positive within-regime cloud amount feedback countered slightly by a negative within-regime optical depth feedback. These within-regime feedbacks are highly uniform: In nearly all regimes, locations, and models, cloud amount decreases and cloud albedo increases with warming. In contrast, global-mean across-regime components vary widely across models but are very small on average. This component, however, is dominant in setting the geographic structure of the shortwave cloud feedback: Thicker, more extensive cloud types increase at the expense of thinner, less extensive cloud types in the extratropics, and vice versa at low latitudes. The prominent negative extratropical optical depth feedback has contributions from both within- and across-regime components, suggesting that thermodynamic processes affecting cloud properties as well as dynamical processes that favor thicker cloud regimes are important. The feedback breakdown presented herein may provide additional targets for observational constraints by isolating cloud property feedbacks within specific regimes without the obfuscating effects of changing dynamics that may differ across timescales.

Keywords Climate sensitivity · Cloud feedback · Cloud regimes

1 Introduction

The responses of clouds to planetary warming—cloud feedbacks—are the primary cause of uncertainties in future warming for a given increase in greenhouse gas concentration. This stems from the large role of clouds in modifying the flow of heat into and out of the Earth system and the challenge of observing, understanding, and modeling cloud

processes at scales ranging from microscopic to global for the wide variety of cloud types and responses to warming that together make up the cloud feedback.

Recent work using cloud radiative kernels (Zelinka et al. 2012a, b, 2013, 2016) has advanced our ability to diagnose cloud feedbacks, providing new insights into robust features simulated by all models, their linkage to the physical processes driving them, and their sources of inter-model spread. For example, it is now clear that models systematically simulate positive feedbacks from decreases in low-cloud amount, positive feedbacks from rising high-cloud top altitude, and negative feedbacks from increases in low-cloud optical depth.

However, as noted in Zelinka et al. (2012a), there remains ambiguity regarding the actual causes of the cloud changes that drive some of these components. For example, climate models robustly simulate a negative feedback from increased optical depth of (primarily) low-level extratropical clouds. This feedback could have contributions from both changes in

✉ Mark D. Zelinka
zelinka1@llnl.gov

¹ Lawrence Livermore National Laboratory, 7000 East Avenue, L-103, Livermore, CA 94550, USA

² McGill University, Room 817, Burnside Hall, 805 Sherbrooke Street West, Montreal, QC H3A 0B9, Canada

³ Earth Sciences Division, NASA/GSFC, Mail Code: 613, MD 20771 Greenbelt, USA

⁴ NASA Goddard Institute for Space Studies, 2880 Broadway, New York, NY 10025, USA

the relative frequency of occurrence of optically thin versus thick cloud types as well as from changes in the optical properties of clouds of a given morphology. In the former case, it is possible that transitions from relatively thin boundary layer clouds to thicker frontal clouds, perhaps associated with a storm-track shift, are leading to the overall increase in cloud albedo. This would imply that a better understanding of changes in meteorology and large-scale dynamics would be necessary to constrain this feedback. In the latter case, optical properties of the cloud types that are already present are changing (e.g., thin boundary layer clouds becoming thicker), suggesting a greater role for thermodynamic processes that increase cloud liquid water content or decrease particle size. While it is likely that some combination of both processes contributes to this and other feedbacks, distinguishing the two would be helpful for interpreting which processes cause the feedback on average, which drive its inter-model spread, and which need attention when determining how to correct biases in models.

Independent of the work done using cloud radiative kernels, novel techniques have allowed for a clear breakdown of cloud feedbacks into components due to changes in the relative frequency of occurrence of various cloud regimes and due to changes in within-regime cloud radiative properties (Williams and Tselioudis 2007; Williams and Webb 2009; Tsushima et al. 2016). These are related to and build on previous work separating tropical cloud regimes into vertical motion regimes, allowing for a clean separation of thermodynamic (within-regime) and dynamic (across-regime) components of cloud feedback (Bony and Dufresne 2005; Bony et al. 1997, 2004). These analyses typically rely on cloud radiative effect (CRE; the difference between clear- and all-sky top of atmosphere radiative fluxes)—a useful but highly integrated measure of how clouds impact radiation. As such, results derived therein do not distinguish changes in, for example, cloud altitude from cloud amount in driving longwave CRE changes in a given regime, or between cloud amount and cloud optical depth in driving shortwave CRE changes in a given regime. It is also unclear how across-regime changes manifest in cloud property feedbacks (e.g., how population shifts between cloud regimes with distinct radiative properties translate into amount, altitude, and optical depth feedbacks).

Hence it is natural to bring together these two techniques to leverage their strengths in detailing complementary aspects of cloud feedback. Cloud regime analysis would illuminate the currently ambiguous processes driving some of the robust yet uncertain cloud feedbacks revealed by kernels, and kernel analysis would illuminate the currently ambiguous changes in specific cloud properties contributing to both dynamic- and thermodynamic-induced feedbacks revealed by regime analysis. This paper thus has two primary goals: The first is to demonstrate that these two techniques can

be jointly applied to climate model data. We present the mathematical basis for our approach of combining these two analysis techniques in Sect. 2. The second is to present some novel insights about cloud feedback that come out of doing this diagnostic analysis, which we do in Sect. 3. With these two goals achieved, we present our conclusions and discuss avenues of future work in Sect. 4.

2 Methodology of combining cloud kernel and cloud regime analyses

At the conceptual level, our analysis is fairly straightforward: We modify the existing cloud regime analysis techniques to operate on joint histograms of cloud-induced radiative anomalies rather than on 2-dimensional cloud radiative effect anomalies. This allows us to derive within- and across-regime changes in cloud-induced radiation anomalies partitioned among the various property changes of interest. A primary technical challenge is that the cloud radiative kernels are defined at monthly resolution, whereas cloud regimes are determined at the daily timescale, so we must assign locations to cloud regimes at the daily scale, average them to monthly, and pair them with cloud radiative kernels corresponding to each month and regime. After that, standard cloud feedback analysis using monthly-resolved data can proceed, now with the additional dependence on cloud regime. In the remainder of the section, we detail these steps.

To begin, note that the value of some cloud-related quantity (X) for any given region can be expressed as a sum over all R regimes of the average X within a regime (X_r), scaled by the relative frequency of occurrence of that regime (f_r):

$$X = \sum_{r=1}^R f_r X_r. \quad (1)$$

Regimes are commonly determined via two approaches: One is to aggregate data into meteorological regimes characterized by certain features of the large-scale circulation, like 500 hPa vertical motion (Bony et al. 1997, 2004), horizontal temperature advection (Norris and Iacobellis 2005), or proximity to cyclones (Tselioudis and Rossow 2006; Bodas-Salcedo et al. 2012, 2014; McCoy et al. 2019, 2020). Another is to determine cloud regimes (sometimes called weather states) by applying semi-objective clustering algorithms to the cloud characteristics themselves, typically joint histograms of cloud fraction segregated by cloud top pressure and optical depth (Jakob and Tselioudis 2003; Gordon et al. 2005; Gordon and Norris 2010; Williams and Tselioudis 2007; Williams and Webb 2009; Oreopoulos and Rossow 2011; Jin et al. 2017a, b; Tsushima et al. 2013, 2016). In this study we use regimes that are defined using the latter approach, described in more detail below.

Table 1 Model variants used in this study, along with their model description references and digital object identifiers for their data published to the Earth System Grid Federation

Model	Variant	References	amip	amip+4K
CNRM-CM5	r1i1p1	Voldoire et al. (2019)	10.1594/WDCC/CMIP5.CEC5am	10.1594/WDCC/CMIP5.CEC5a4
HadGEM2-A	r1i1p1	Collins et al. (2011)	10.1594/WDCC/CMIP5.MOGAam	10.1594/WDCC/CMIP5.MOGAa4
MIROC5	r1i1p1	Watanabe et al. (2010)	10.1594/WDCC/CMIP5.MIM5am	10.1594/WDCC/CMIP5.MIM5a4
MPI-ESM-LR	r1i1p1	Stevens et al. (2013)	10.1594/WDCC/CMIP5.MXELam	10.1594/WDCC/CMIP5.MXELa4
MRI-CGCM3	r1i1p1	Yukimoto et al. (2012)	10.1594/WDCC/CMIP5.MRMCam	10.1594/WDCC/CMIP5.MRMCa4
CanESM5	r1i1p2f1	Swart et al. (2019)	10.22033/ESGF/CMIP6.3535	10.22033/ESGF/CMIP6.3548
CNRM-CM6-1	r1i1p1f2	Voldoire et al. (2019)	10.22033/ESGF/CMIP6.3922	10.22033/ESGF/CMIP6.3938
HadGEM3-GC31-LL	r5i1p1f3	Williams et al. (2018)	10.22033/ESGF/CMIP6.5853	10.22033/ESGF/CMIP6.5873
IPSL-CM6A-LR	r1i1p1f1	Boucher et al. (2020)	10.22033/ESGF/CMIP6.5113	10.22033/ESGF/CMIP6.5126
MRI-ESM2-0	r1i1p1f1	Yukimoto et al. (2019)	10.22033/ESGF/CMIP6.6758	10.22033/ESGF/CMIP6.6771

The first five models listed are from CMIP5 and the latter are from CMIP6

Anomalies in X with respect to some base state can be expressed as

$$\Delta X = \sum_{r=1}^R (f_r \Delta X_r + \Delta f_r X_r + \Delta f_r \Delta X_r), \tag{2}$$

where the terms on the right-hand side (RHS) are the components due to changes in the within-regime cloud property, changes in the relative frequency of occurrence of each regime, and a covariance term. If X is cloud radiative effect and these anomalies are normalized by the global mean temperature change (e.g., between a perturbed and control climate model experiment), these terms represent three components of the cloud feedback, albeit a biased measure in the presence of clear-sky flux changes (Soden et al. 2004, 2008). These terms have been diagnosed and investigated in climate models in several studies (Williams and Tselioudis 2007; Williams and Webb 2009; Tsushima et al. 2016). Here we use Atmospheric Model Intercomparison Project simulations in which observed sea surface temperatures (SSTs) and sea ice concentrations are prescribed to match observations, known as `amip` experiments. For the climate change response, we use similar atmosphere-only experiments, but the prescribed SSTs are uniformly increased by 4 K over the ice-free oceans. These perturbed experiments are known as `amip4K` in CMIP5 (Taylor et al. 2012) and `amip-p4K` in CMIP6 (Eyring et al. 2016). We will hereafter refer to these perturbed experiments as `amip+4K`.

For each model and for the `amip` and `amip+4K` experiments, we use daily-resolution surface air temperature, surface upwelling and downwelling clear-sky SW fluxes, and the following fields that are produced by the ISCCP simulator (Klein and Jakob 1999; Webb et al. 2001): cloud fractions reported in joint cloud top pressure/visible optical depth histograms (C), along with grid-box mean cloud albedo (α_c), cloud top pressure (p_c), and total cloud cover

(C_{tot}). The latter three fields are computed ignoring clouds with optical depths less than 0.3, the minimum detection threshold of ISCCP. Necessary model diagnostics from both `amip` and `amip+4K` experiments are available from five CMIP5 models and five CMIP6 models (Table 1).

For the reasons discussed in Williams and Webb (2009), we assign each daily GCM grid point to a specific cloud regime by finding the minimum Euclidean distance between the models' [α_c, p_c, C_{tot}] vector at that grid point and that of the observed centroids. The observed regimes to which we assign model data are the eight global weather states derived from ISCCP-H observations (Tselioudis et al. 2021). The mean values of the three cloud properties for each centroid are given in Table 2 of Tselioudis et al. (2021), except cloud optical depth rather than albedo is reported. We convert centroid-mean cloud optical depth (τ_c) to cloud albedo (α_c) using the analytic formula:

$$\alpha_c = \tau_c^{0.895} / (\tau_c^{0.895} + 6.82), \tag{3}$$

which approximates the ISCCP lookup tables relating grid-mean albedo to grid-mean cloud optical thickness (Table 3.1.2 of Rossow et al. 1996), and is used by the ISCCP simulator to compute grid-box mean cloud albedo.

Before computing Euclidean distances, we normalize the α_c , p_c , and C_{tot} values by their respective standard deviations, following Jin et al. (2017a). The standard deviation is calculated across a concatenated vector of all grid points and all days over the period 2003–2005 in the `amip` experiment of each model. This normalization is necessary because the three fields have different units, and is done to both the modeled and observed fields to ensure that the observational centroids are properly projected into model space. The process of regime assignment yields a binary occurrence matrix (n) that is a function of regime (r), day (d), latitude (ϕ), and longitude (θ) containing ones

where that location belongs to a given regime and zeros where it does not.

Cloud radiative kernels are a function of month, p_c , τ_c , latitude, and—in the case of the SW kernel—clear-sky surface albedo (α_{clr}). In order to compute feedbacks we need to aggregate the daily data to monthly resolution and map the SW kernel from its native α_{clr} space to longitude¹. For each regime and grid point, we determine the appropriate SW kernel based on the mean clear-sky surface albedo for that regime and grid point. First we compute monthly-averaged climatologies of the data segregated by regime (X_r) as the n -weighted average of daily data (x) over all days (d) in each of the 12 calendar months (m) over the same 9-year portion of the amip and amip+4K simulations:

$$X_r(m, \phi, \theta) = \frac{1}{N_r} \sum_{y=2000}^{2008} \sum_{d=1}^{D(m_y)} x(d, \phi, \theta) * n_r(d, \phi, \theta), \quad (4)$$

where $D(m_y)$ is the total number of days within month m of year y , and N_r is the total number of occurrences of each regime in each month and at each location, computed as:

$$N_r(m, \phi, \theta) = \sum_{y=2000}^{2008} \sum_{d=1}^{D(m_y)} n_r(d, \phi, \theta). \quad (5)$$

The results presented hereafter are not sensitive to the number of years or the choice of years analyzed, but geographically-resolved results are less noisy as more years are included. The above process is performed for the cloud fraction histogram (in which case x and X_r additionally have dimensions of p_c and τ_c) and clear-sky surface albedo (α_{clr}). The resultant monthly- and regime-resolved α_{clr} is then used to determine the appropriate SW cloud radiative kernel. This is the same process as described in Zelinka et al. (2012b), except here we transform the kernel from its native latitude- α_{clr} space to latitude-longitude space for each regime, based on $\alpha_{clr}(m, \phi, \theta)$ for each regime. (This step is not needed for the LW kernels since they depend only on latitude and not on α_{clr} .) Hence for each month and location, each cloud regime has its own SW kernel that is appropriate for the average α_{clr} present on the days within the month assigned to that regime. Finally, we define the relative frequency of occurrence (f_r) as the fraction of days within a month that a regime is present at a given location:

$$f_r(m, \phi, \theta) = \frac{N_r(m, \phi, \theta)}{\sum_{r=1}^R N_r(m, \phi, \theta)}. \quad (6)$$

The sum of f_r over all regimes equals 1 for that location. Hereafter we drop the notation specifying that regime-segregated quantities are additionally functions of month, latitude, and longitude.

This analysis yields climatological cloud fraction histograms (C_r), cloud radiative kernel histograms (K_r), and relative frequency of occurrences (f_r) that are segregated into 8 cloud regimes at each latitude and month, for both the amip and amip+4K experiments. A 9th clear-sky regime where $C_{tot} = 0$ is also tracked. Replacing X_r with the product of C_r and K_r in Eq. (2), we can now express the cloud feedback as:

$$\lambda_{cld} = \frac{1}{\Delta T_s} \sum_{r=1}^R K_r (f_r \Delta C_r + \Delta f_r C_r + \Delta f_r \Delta C_r), \quad (7)$$

where T_s is the global mean surface air temperature, Δ refers to the difference between amip+4K and amip climatologies, and any field without a Δ preceding it refers to the amip climatology.

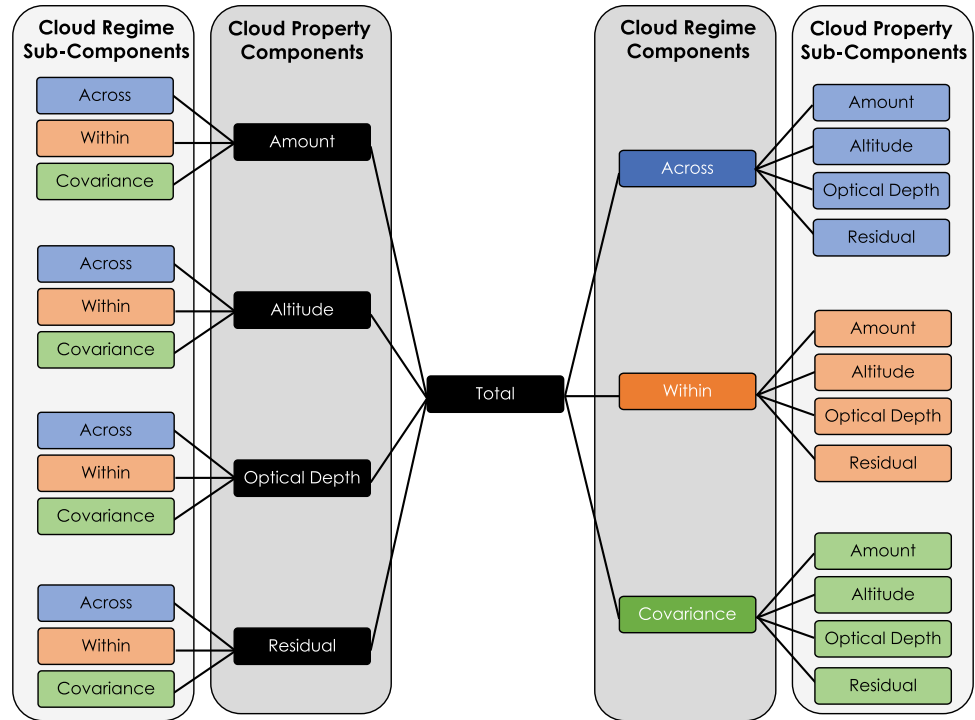
The key novelty of our analysis is that X_r in (2) is replaced with $C_r K_r$ in (7), where C_r and K_r are additionally functions of cloud top pressure and visible optical depth, giving us the ability to further break these terms down into components due to individual cloud property changes, something which cannot be done if X refers to CRE. We will now discuss this break down in greater detail.

The first term on the RHS of Eq. 7 ($f_r \Delta C_r K_r$) is the cloud feedback arising from changes in within-regime cloud properties, and the third ($\Delta f_r \Delta C_r K_r$) is the covariance term. Both of these naturally break down into amount, altitude, and optical depth components (Zelinka et al. 2012a, 2013). As shown below the covariance term is generally very small.

The second term on the RHS of Eq 7 is the cloud feedback arising from changes in the relative frequency of occurrence of each regime. Because it is simply the product of a scalar change in regime RFO (Δf_r), the control climate cloud histogram (C_r), and the radiative kernel (K_r), it can only manifest as an amount feedback. (The altitude and optical depth components are identically zero because this product implies a change only in total cloud amount rather than in the p_c or τ_c distribution.) However, it is desirable to quantify cloud property feedbacks due to changes in the frequency of occurrence of regimes with different properties. For example, we would like to quantify the optical depth feedback arising from shifts from thinner-than-average to thicker-than-average regimes, which would be embedded in this second term. To do so, we express this term as the sum of four components:

¹ Note that we can alternatively use the daily clear-sky surface albedo to map the kernels from albedo to longitude space and then assign this daily- and spatially- resolved kernel to the appropriate cloud regime at every grid point prior to aggregating everything to monthly resolution. So doing requires assuming that the radiative kernel from a given month is applicable to each day within that month. Performing the analysis in this manner results in identical results as shown hereafter.

Fig. 1 Schematic of the cloud feedback decomposition. We decompose the total cloud feedback into cloud regime components (within-regime, across-regime, and covariance terms), which are further broken down into cloud property sub-components (amount, altitude, optical depth, and residual terms). These resulting cloud property sub-components are re-organized on the left branch of the diagram such that each cloud regime sub-component is grouped by cloud property component. Feedback sub-components on the left- and right-most branches with the same colors are identical, but simply organized differently to aid complementary interpretations



$$\Delta f_r C_r K_r = \Delta f_r (\overline{CK} + \overline{CK}'_r + C'_r \overline{K} + C'_r K'_r), \tag{8}$$

where \overline{C} is the annual- and regime-averaged histogram at each location, and $C'_r = C_r - \overline{C}$ contains all monthly- and regime-dependent deviations of the histogram from this. K'_r and \overline{K} are defined in the same manner. Note that the regime average quantities and deviations therefrom are computed only considering the regimes with nonzero cloud fraction and that the cloud fraction of clear-sky Regime 9 is fixed to zero. Of these terms, the third ($\Delta f_r C'_r \overline{K}$) turns out to be dominant when results are summed over all regimes (SI Fig. 1). This makes sense because regimes defined by clustering cloud fraction histograms essentially guarantees that across-regime variations in climatological cloud fraction histograms are substantial. These variations are much larger than across-regime variations in kernels (term 2) or their covariances (term 4). Moreover, since the across-regime sum of Δf_r is zero by definition, the across-regime sum of a scalar (\overline{CK}) times Δf_r (term 1) must also be zero. Therefore, we can express Eq. 8 as:

$$\Delta f_r C_r K_r = \Delta f_r C'_r \overline{K} + \epsilon, \tag{9}$$

which leads to our ultimate expression for the cloud feedback breakdown:

$$\lambda_{cld} = \frac{1}{\Delta T_s} \sum_{r=1}^R (\Delta f_r C'_r \overline{K} + f_r \Delta C_r K_r + \Delta f_r \Delta C_r K_r + \epsilon). \tag{10}$$

We shall hereafter refer to these first three components as the “across-regime”, “within-regime”, and “covariance” components. As will be shown below (and in SI Fig. 1), the neglected “across-regime” components encapsulated in ϵ are small. A schematic illustrating the complete break-down of cloud feedback produced in this study is shown in Fig. 1.

The analysis is performed for LW, SW, and net (LW+SW) cloud feedbacks, but for the sake of simplifying the presentation of results, we will focus hereafter on just the SW cloud feedback. LW and net cloud feedback results will be analyzed in future work.

3 Results

3.1 Cloud regime characteristics

Multi-model mean cloud fraction histograms averaged within each of the cloud regimes and maps showing the relative frequency of occurrence of each cloud regime are shown in Figs. 2 and 3, respectively. Global-mean values of total cloud cover, albedo, cloud top pressure, and relative frequency of occurrence for each regime averaged across all models (and their across-model standard deviation) are provided in Table 2. Comparing these figures with their observational counterparts shown in Figure 1 of Tselioudis et al. (2021), we see many qualitative similarities, as expected given that we are matching modeled cloud properties to the observed centroids, as well as some noteworthy differences.

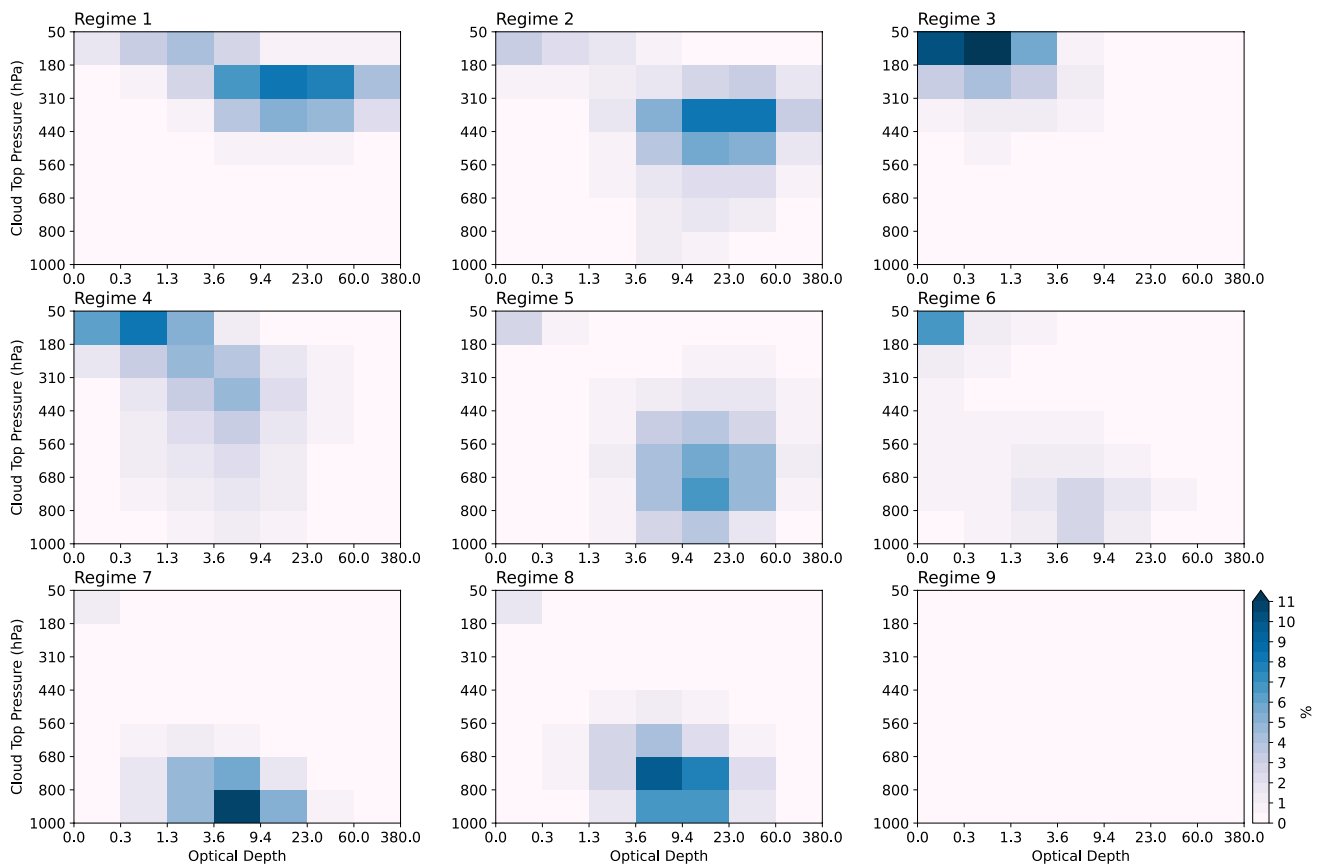


Fig. 2 Cloud fraction histograms for each regime, averaged across models and globally

Regime 1 contains primarily high, thick clouds and is prevalent in regions of tropical deep convection, similar to observations. Regime 2 contains moderately thick high clouds (as well as some lower clouds) that are prevalent in the middle-latitude storm-track region. Unlike in the observations, this regime is not confined to middle latitudes and also occurs frequently in tropical ascent regions in the models. Regime 3 is a cirrus cloud category, with very high thin clouds that are prevalent in the Indo-Pacific warm pool region, but also over subtropical land regions, similar to observations. Regime 4 contains a broad range of cloud top pressures and optical thicknesses but is dominated by high, relatively thin clouds, similar to the observations. Unlike in observations, however, this regime occurs frequently outside of the polar regions, including in tropical ascent regions. Given that it is a high cloud regime with average total cloud cover and albedo lying between the values of the other high cloud regimes (Regimes 1–3), we refer to it as a ‘hybrid high’ cloud regime. Optically thick mid-level clouds that are prevalent over the middle latitude oceans characterize Regime 5, in qualitative agreement with the observations. Unlike the observations, the regime occurs often in the East Pacific ITCZ region, and the overall frequency of occurrence is roughly twice as large as in

observations. As in observations, Regime 6 is the most frequently observed regime (RFO of nearly 40%), and contains a mix of scattered thin cumulus and cirrus clouds, with generally small cloud fractions. It is most prevalent over trade cumulus regions. Regimes 7 and 8 are dominated by low clouds that are prevalent over cold sea surface temperatures, as in observations. Regime 7 contains lower-topped, slightly thinner clouds with smaller fractional coverage than Regime 8, which led Tselioudis et al. (2021) to classify these as shallow cumulus and stratocumulus clouds, respectively. Unlike in observations where these two regimes occur with similar frequency, the RFO of Regime 8 is three times greater than that of Regime 7 in the model mean. Regime 9 is the clear-sky regime, which is prevalent over the subtropical continents and Antarctica. Its geographic distribution and global mean RFO are very similar to observations.

Some of the model-observation discrepancies mentioned above may be alleviated by performing the minimum Euclidean distance calculation with the full information content of the histograms (Williams and Tselioudis 2007) rather than the simplified 3-element vector (Williams and Webb 2009), though we have not tested this. However, this paper is not concerned with evaluating

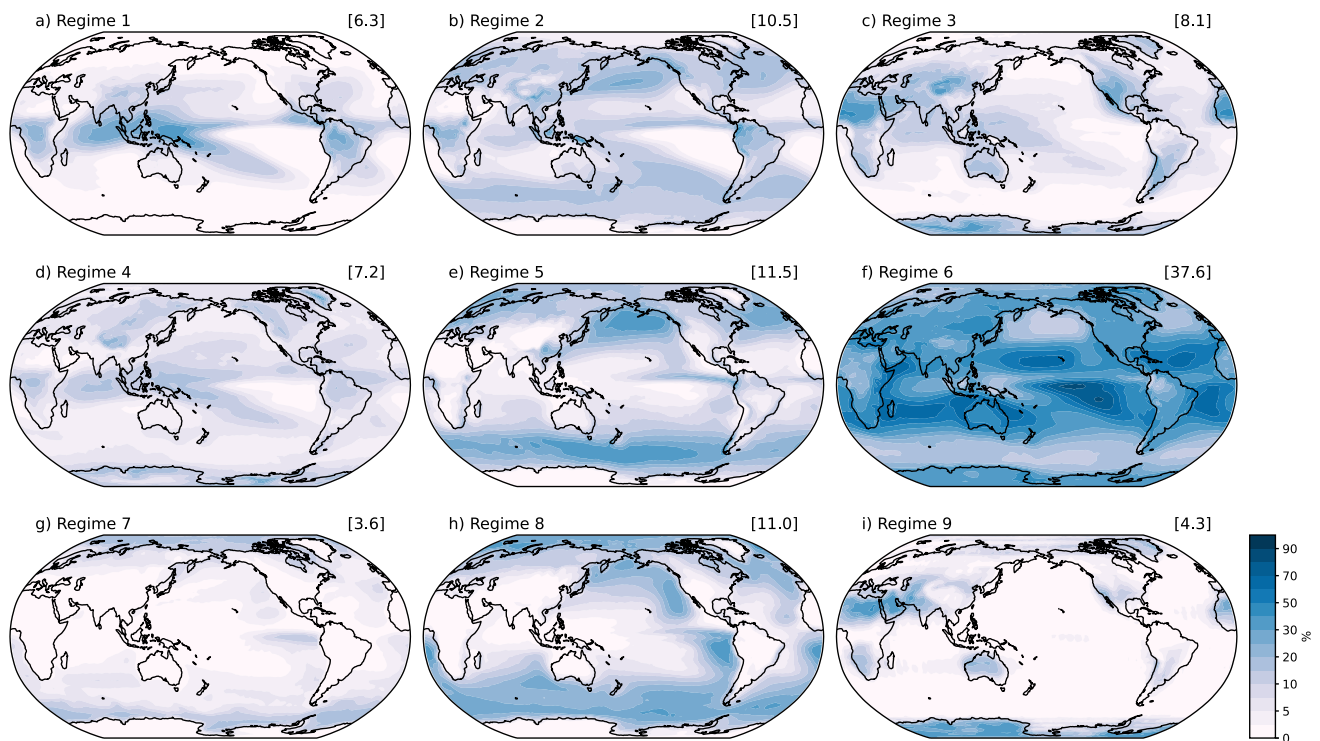


Fig. 3 Relative frequency of occurrence of each regime, expressed as a percentage of time that a given regime is present at each grid point, averaged across models. The global average RFO is displayed in the title of each panel

Table 2 Multi-model mean global mean total cloud cover (C_{tot}), cloud albedo (α_c), cloud top pressure (p_c), and relative frequency of occurrence (RFO) of each regime in the control climate

Regime	Description	C_{tot} [%]	α_c [%]	p_c [hPa]	RFO [%]
1	Tropical deep convection	83.8 (9.7)	54.7 (2.7)	281.7 (14.6)	6.3 (1.5)
2	Midlatitude storm track	80.9 (4.5)	57.8 (3.6)	429.9 (6.2)	10.5 (3.2)
3	Optically thin cirrus	42.8 (8.5)	18.8 (2.0)	239.8 (23.3)	8.1 (2.9)
4	Hybrid high	68.4 (6.6)	32.2 (1.7)	369.2 (17.8)	7.2 (2.5)
5	Optically thick mid-level	75.4 (5.5)	57.9 (3.3)	615.3 (15.5)	11.5 (4.1)
6	Scattered thin cumulus & cirrus	26.6 (4.0)	37.4 (4.7)	648.5 (41.4)	37.6 (7.4)
7	Shallow cumulus	61.6 (4.9)	39.3 (3.8)	805.2 (25.2)	3.6 (1.5)
8	Stratocumulus	71.1 (6.0)	48.6 (3.9)	723.5 (26.1)	11.0 (3.2)
9	Clear-sky	0.0 (0.0)			4.3 (3.3)

The 1- σ range across models is shown in parenthesis

models’ ability to simulate the correct within-regime cloud characteristics or the correct frequency of occurrence of the various regimes. Such model evaluation studies have already been done previously, including for the regimes used in this study (Tselioudis et al. 2021). Our objective, rather, is to demonstrate the utility of employing a regime framework to better understand the processes driving cloud feedbacks, allowing us to distinguish within- from across-regime cloud changes in contributing to the various cloud property feedbacks, and vice versa. Such an analysis does not require that models’ cloud regime properties match observations particularly well, only that their clouds

can be grouped into a set of regimes with reasonably-distinct and physically-interpretable characteristics that facilitates such a breakdown. The attribution of across-regime changes to large-scale atmospheric dynamics is supported by the fact that the cloud regimes show skill in tracing distinct meteorological states and cloud formation mechanisms, as demonstrated in Tselioudis et al. (2021). As will be demonstrated below, our breakdown is not sensitive to the exact definition of regimes. Hence the results are resilient to reasonable variations in how exactly the regimes are initially defined.

Table 3 As in Table 2, but showing the response to +4K warming for each regime

Regime	Description	ΔC_{tot} [%/K]	$\Delta \alpha_c$ [%/K]	Δp_c [hPa/K]	ΔRFO [%/K]
1	Tropical deep convection	-0.28 (0.47)	0.24 (0.17)	-3.06 (0.94)	0.36 (0.24)
2	Midlatitude storm track	-0.69 (0.35)	0.27 (0.15)	-0.48 (0.53)	0.02 (0.09)
3	Optically thin cirrus	-0.07 (0.23)	0.19 (0.09)	-3.21 (1.17)	0.14 (0.16)
4	Hybrid high	-0.51 (0.27)	0.15 (0.07)	-3.39 (1.17)	-0.18 (0.10)
5	Optically thick mid-level	-0.61 (0.16)	0.29 (0.10)	0.69 (0.99)	0.07 (0.22)
6	Scattered thin cumulus and cirrus	-0.28 (0.21)	0.35 (0.11)	-0.89 (1.20)	0.12 (0.38)
7	Shallow cumulus	-0.28 (0.15)	0.16 (0.06)	-0.14 (0.65)	-0.23 (0.17)
8	Stratocumulus	-0.49 (0.19)	0.18 (0.10)	-0.00 (0.70)	-0.32 (0.21)
9	Clear-sky	0.00 (0.00)			0.03 (0.15)

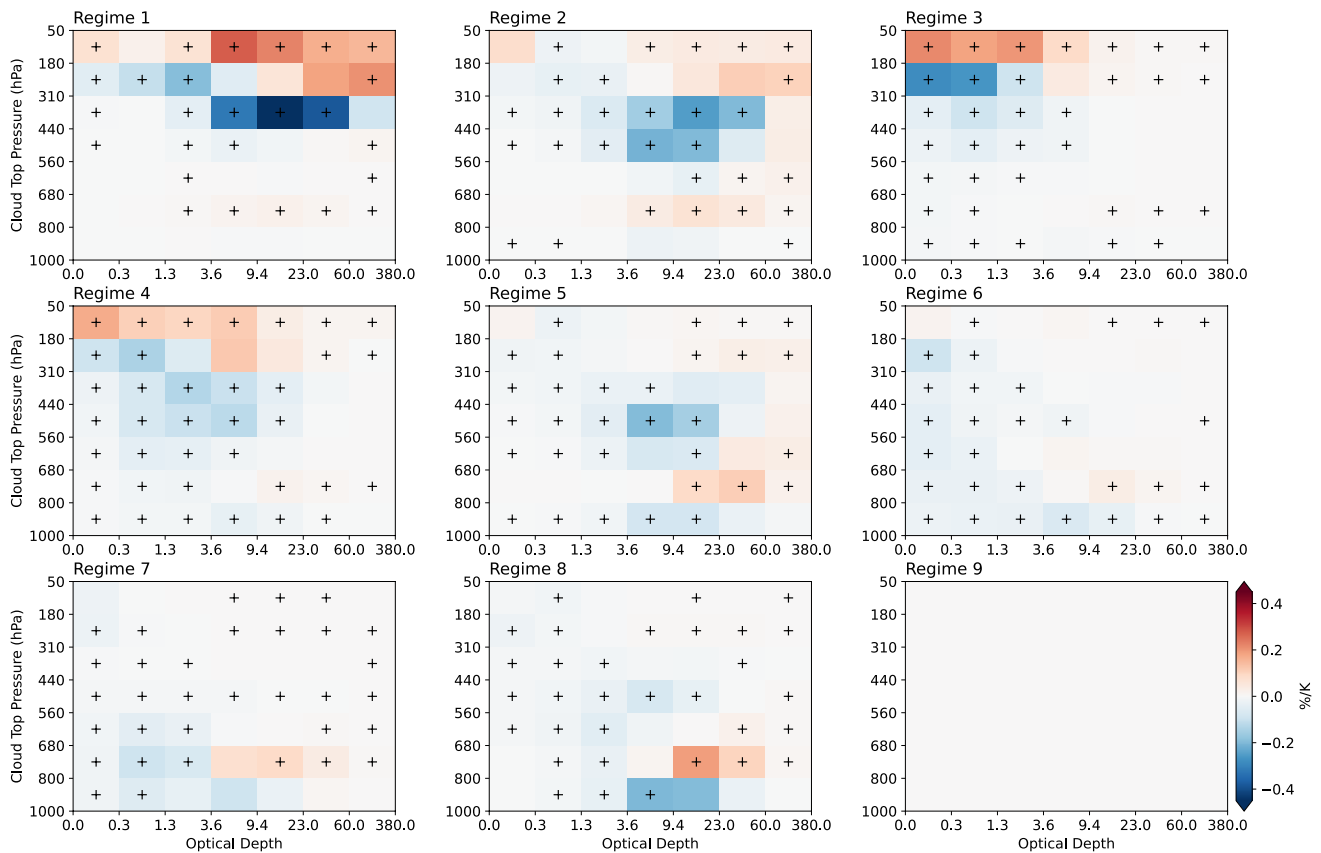


Fig. 4 Temperature-mediated change in cloud fraction histograms for each regime, averaged across models and globally. Stippling indicates locations where at least 8 out of 10 models agree on the sign of the change (not shown for clear-sky Regime 9)

3.2 Changes in regime-averaged properties

To aid in interpreting the feedback results shown below, in Fig. 4 we show the change in the regime-averaged cloud fraction histograms under +4K warming, averaged across the 10 models analyzed (Table 1). Table 3 shows changes in globally-averaged cloud properties in each regime, averaged across models. In all regimes, the cloud fraction decreases for mid-level clouds of most thicknesses and for clouds with highest cloud top pressures (i.e., nearest to the surface).

The fraction of clouds at the highest altitudes increases, most notably in regimes dominated by high clouds (Fig. 4, Regimes 1–4). This, coupled with the strong decreases in cloud fractions at levels immediately below, indicates an upward shift of cloud tops. This upward shift has a theoretical basis in the fixed anvil temperature hypothesis which states that high cloud tops will rise so as to remain at an approximately fixed temperature as the troposphere deepens with warming (Hartmann and Larson 2002; Thompson et al. 2017). In addition to being robustly simulated in

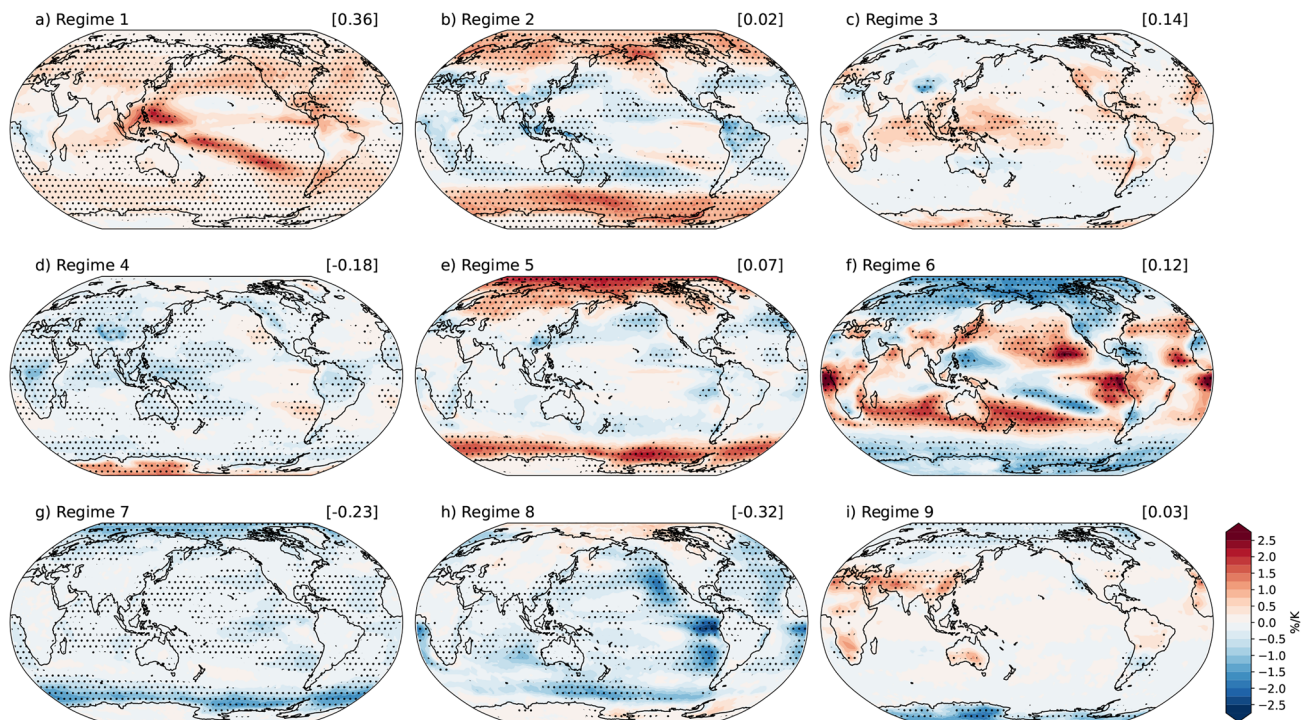


Fig. 5 Temperature-mediated change in the relative frequency of occurrence of each regime, averaged across models. The global average RFO change is displayed in the title of each panel. Stippling indicates locations where at least 8 out of 10 models agree on the sign of the change

global climate models, it is also simulated in high resolution models, and has been observed in response to climate variability and secular trends (Sherwood et al. (2020) and references therein). Cloud fraction increases are also apparent between 680 and 800 hPa in most regimes, but most prominently in the cumulus and stratocumulus regimes (Fig. 4, Regimes 7 and 8). In all regimes, these increases occur immediately above bins with similar decreases, again suggesting an upward shift of the low-level cloud population with warming.

Aside from the aforementioned changes in cloud top altitude, two other gross cloud properties exhibit systematic changes with warming: In every regime, total cloud fraction decreases and optical depth increases. The former is difficult to discern directly from the histograms, but is indicated by the change in total cloud fraction shown in Table 3. The latter can be inferred from the overall tendency for an increase in cloud fraction in higher optical depth bins of the histograms along with corresponding decreases in cloud fraction in the thinner bins, and verified in the $\Delta\alpha_c$ column of Table 3. Hence, for clouds of a given regime, warming causes them to systematically rise, increase in albedo, and decrease in coverage. As will be seen below, this leads to within-regime cloud feedback components that are highly consistent across models and across regimes.

The change in regime relative frequency of occurrence maps is shown in Fig. 5, and in Fig. 6 we show the

zonal-mean RFO and its change. The RFO of high cloud regimes 1 and 3 increases systematically, most prominently where these regimes are prevalent climatologically. Regimes 4, 7, and 8 all show large decreases in RFO at nearly all latitudes, with the latter being especially prominent in the eastern ocean basins in Regime 8. These decreases in the RFO of Regimes 7–8 coincide with prominent increases in the RFO of Regime 6, highly suggestive of a stratocumulus-to-cumulus transition.

Comparing Figs. 3 and 5, and panels (a) and (b) of Fig. 6, one can discern poleward shifts of cloud types. This is apparent for Regimes 2 and 5, for which increases in RFO occur at latitudes just poleward of the control-climate RFO maximum, where RFO is strongly decreasing with latitude. The opposite response is also apparent at locations just equatorward of the control-climate RFO maximum. Both of these regimes correspond to storm-track clouds, which are expected to shift poleward with warming (Yin 2005; Barnes and Polvani 2013). Similarly, increases in the RFO of Regime 6 peak near 40°S and 40°N, where its control-climate RFO falls off rapidly with latitude. This is suggestive of a poleward expansion of the subtropics and of the already-ubiquitous cumulus regime.

Overall, the cloud population tends to shift from cloudier and thicker regimes (2, 5, and 8) towards less-cloudy and thinner regimes (3 and 6) at low latitudes, with the opposite response in the extratropics. Put another way, the regimes

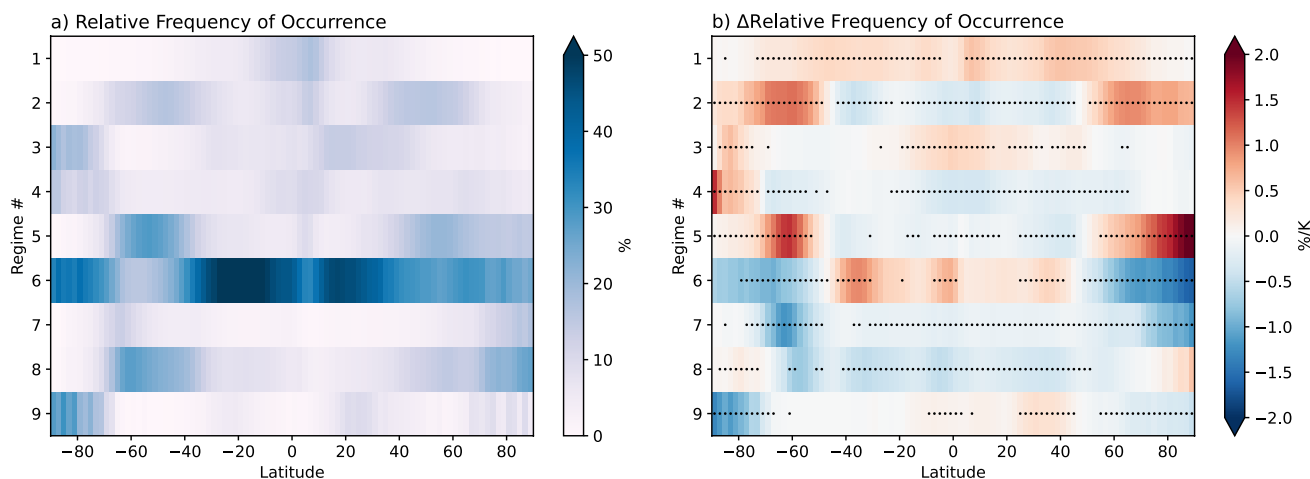


Fig. 6 **a** Zonally averaged relative frequency of occurrence of each cloud regime, averaged across models, and **(b)** its temperature-mediated change in response to +4K warming. Stippling in **(b)** indicates locations where at least 8 out of 10 models agree on the sign of the change

characterized by bright and extensive clouds shift poleward with warming, and in their wake the conditions are favorable for regimes characterized by thinner and less extensive clouds.

3.3 Global mean feedback decomposition

As mentioned above, the cloud feedback has previously been broken down into within-regime, across-regime, and covariance terms (Williams and Tselioudis 2007; Williams and Webb 2009; Tsushima et al. 2016), but these have not been further segregated into their amount, altitude, and optical depth sub-components. Likewise, the previously-diagnosed amount, altitude, and optical depth feedback components (Zelinka et al. 2012b, 2013, 2016) have not been further broken down into their within, across, and covariance sub-components. In Fig. 7 we perform this more extensive breakdown for the global-mean SW cloud feedback.

At the center of the figure is the true global mean SW cloud feedback computed without performing any breakdown, labeled as “No Breakdown”. The four columns to the left (a–d) provide the cloud property breakdown of this feedback, which are further broken down into cloud regime sub-components and their sum. The four columns to the right (e–h) provide the same information, but organized differently: the cloud regime breakdown of the feedback, further broken down into cloud property sub-components and their sum. (The kernel residual term is not shown because it is very small in all cases.)

Consider first Fig. 7e, which shows the sum of all terms in Eq. 10 except the ϵ term. That the first sub-column within this category (“Total”) closely matches the “No Breakdown” results indicates that the neglected ϵ terms are small and that we can successfully interpret the across-regime component

as primarily being due to $\Delta f_r C_r \bar{K}$ in Eq. 8. This also allows us to break this across-regime component into amount, altitude, and optical depth terms, which are shown in Fig. 7g and discussed below. The global mean SW cloud amount component is robustly positive across the 10 models analyzed, while the altitude component is unsurprisingly small with little inter-model spread (Fig. 7e). The optical depth component is negative in all but two models, with a multi-model average that is smaller in magnitude than that of the amount component, leading to the overall positive multi-model mean SW cloud feedback.

The within-regime component (Fig. 7f) is robustly positive across models, and is made up of two robust feedbacks of opposite sign: a robustly positive amount component and a smaller optical depth component that is negative in all but two models. The within-regime component of the total cloud feedback, as well as its cloud property sub-components, are remarkably similar to those of the total cloud feedback (compare panels e and f). This is especially true for the multi-model mean results, whereas the inter-model spread of the within-regime components are reduced relative to the full feedback. Hence, for the multi-model mean, one can largely attribute the total overall SW cloud feedback and its cloud property sub-components to within-regime cloud changes. This may indicate that—once obfuscating effects of changes in large-scale dynamics are removed—the temperature-mediated response of clouds is very systematic across models. That is, within distinct cloud regimes or weather states, warming causes a systematic decrease in the fractional coverage of clouds—a positive amount feedback—and a systematic increase in the albedo of clouds—a negative optical depth feedback in the vast majority of models. Below we will further show that this uniformity in sign of the within-regime amount and optical depth components

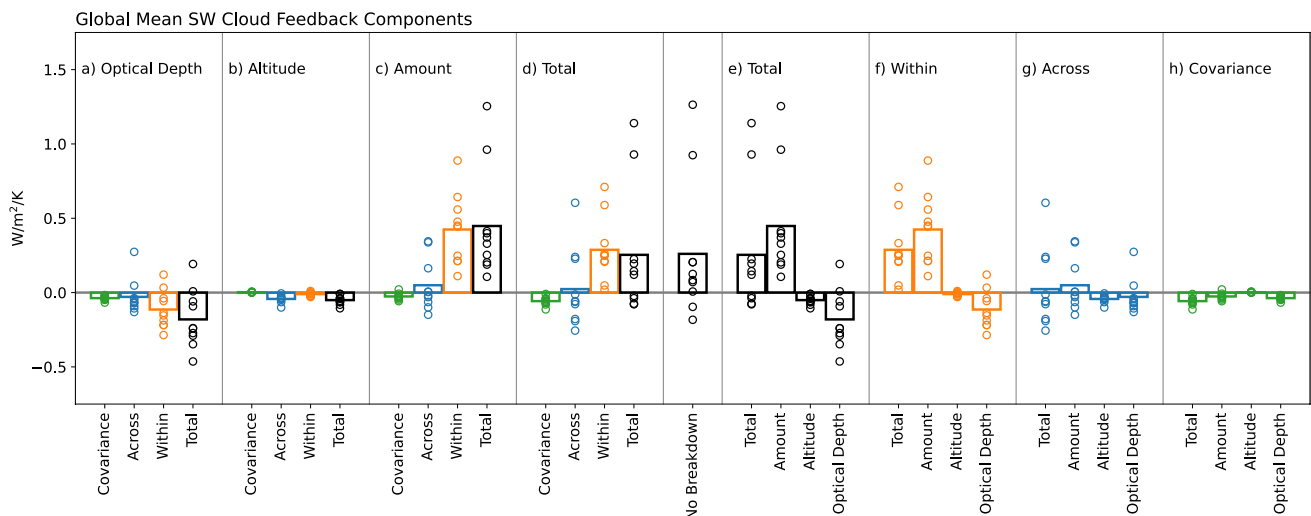


Fig. 7 Globally averaged SW cloud feedbacks for each model, broken down into cloud property and cloud regime components. The “No Breakdown” cloud feedback, which is computed without performing any regime decomposition, serves as a ground-truth for the sum of components that are shown to the left and right. Results are identical

to the left and right of the center column, but organized differently to facilitate complementary comparisons. Columns (a–d) show cloud property components along with the cloud regime sub-components comprising them, while columns (e–h) show cloud regime components along with the cloud property sub-components comprising them

holds not just across models in the global mean sense, but also geographically and across regimes.

In contrast to the within-regime component, the across-regime component exhibits substantial spread across models but with a multi-model mean value that is very close to zero (Fig. 7g, “Total” sub-column). Similarly, the cloud property sub-components of the across-regime feedback exhibit substantial inter-model variations that straddle zero, leading to near-zero contributions to the multi-model average total cloud feedback. This indicates that, averaged over the entire planet, shifts among cloud types (likely caused by changes in large-scale meteorology) can cause large feedbacks of either sign in models, but averaged across all models, these shifts make essentially no contribution to the global, ensemble mean feedback.

In several models, however, the magnitude of the global-mean across-regime component is comparable or even larger than the within-regime component. Both the within- and across-regime SW cloud feedback components are well-correlated with the total global-mean SW cloud feedback across models (not shown). This correspondence extends to both the amount and optical depth sub-components. Hence, although the multi-model mean feedback is primarily attributable to the within-regime component, the inter-model spread in the global mean SW cloud feedback is driven by both the across- and within-regime components. Moreover, as will be shown below, the across-regime component can be very important locally, where shifts among cloud regimes with different properties cause substantial radiative impacts, often of larger magnitude than the within-regime

component. These local contributions can either reinforce or counteract the local within-regime contributions.

The global mean covariance terms (Fig. 7h) are very small, as expected, and will not be discussed further.

Turning to the left four columns of Fig. 7, we see the same information, but re-organized so as to better illuminate how within- and across-regime changes contribute to each of the cloud property feedback components—information that was not revealed in previous studies performing this decomposition (e.g., Zelinka et al. (2012a, 2013, 2016)).

From Fig. 7d, it is clear that the total cloud feedback, on average across models, is entirely coming from the systematically positive within-regime component. The across-regime component, in contrast, can be large and of either sign in models, but averages to a near-zero value across models. The SW cloud amount feedback is robustly positive in all models, with a large multi-model mean (Fig. 7c). Again, this comes almost entirely from the within-regime component, which is systematically positive in all models but with inter-model spread that is smaller than the total amount component. The across-regime cloud amount feedback varies widely among models but is close to zero on average across models. Owing to the weak dependence of reflected SW radiation on cloud top pressure, the SW altitude feedback and all of its sub-components are very small (Fig. 7b). As previously mentioned, the optical depth feedback is negative in all but two models and is moderately negative on average across models (Fig. 7a, “Total” sub-column). The multi-model mean value comes solely from the within-regime component, whereas the across-regime component is close to zero.

From these global mean results, we conclude that, for any given model, both the within-regime and across-regime components can be substantial. However, their roles in the multi-model mean feedback are rather different: The across-regime components tend to exhibit substantial inter-model spread that straddles zero, leading to a multi-model contribution that is negligible. In contrast, the within-regime components tend to be of uniform sign across models (systematically positive for cloud amount and nearly systematically negative for cloud optical depth), such that they are the primary contributor to the positive ensemble-mean SW cloud feedback. Hence a robust signal of temperature-mediated cloud behavior across models becomes apparent when controlling for changes in large-scale meteorology, and one can attribute the positive multi-model mean SW cloud feedback to a robustly positive within-regime SW cloud amount feedback that is partially counteracted by a nearly robustly negative within-regime SW cloud optical depth feedback.

Because the covariance and altitude components have been shown here to be small, we will focus hereafter on the amount and optical depth cloud property components and on the within- and across-regime components so as to simplify the number of fields to consider.

3.4 Spatial structure of the multi-model mean SW cloud feedback and its components

The complementary views of the multi-model mean cloud feedback provided by the marriage of regime-based and kernel-based decompositions are exemplified in Fig. 8. The total SW cloud feedback (a) is broken down in column 1 into its amount (d) and optical depth (g) components, and in row 1 into its across-regime (b) and within-regime (c) components. Note that the global mean value shown in (a) equals the sum of global mean values shown in (b) and (c), plus the covariance term which is not shown. It also equals the sum of global mean values shown in (d) and (g), plus the altitude and kernel residual terms which are not shown because they

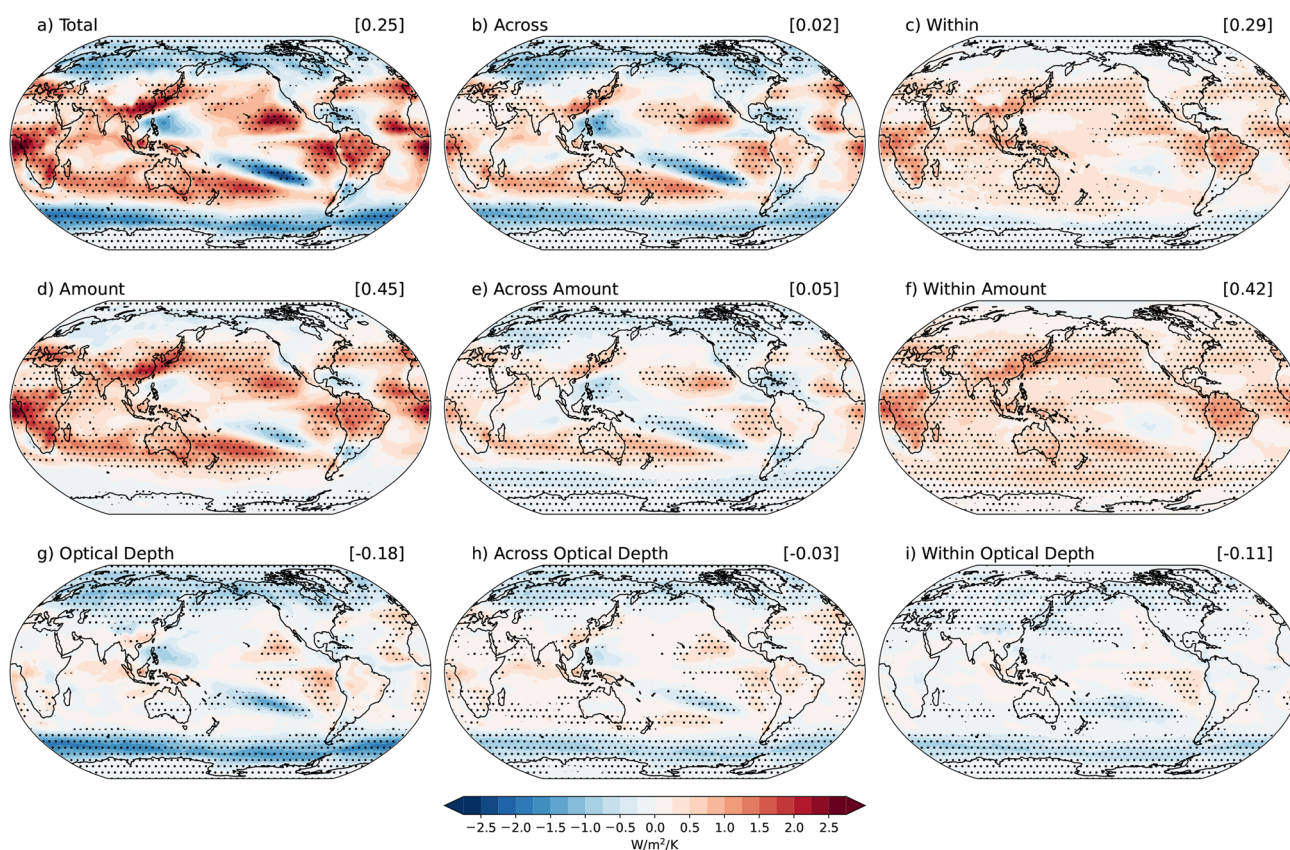


Fig. 8 a Multi-model mean total SW cloud feedback and its breakdown into the dominant terms comprising it; **b** and **c** show the across-regime and within-regime components, while **d** and **g** show the amount and optical depth components. The amount component (**d**) is broken down into its across-regime and within-regime sub-com-

ponents in (**e**) and (**f**), respectively. The optical depth component (**g**) is broken down into its across-regime and within-regime sub-components in (**h**) and (**i**), respectively. Stippling indicates locations where at least 8 out of 10 models agree on the sign of the change

are negligibly small. The across- and within-regime components are broken down into their amount and optical depth sub-components in columns 2 and 3, respectively. Equivalently, the amount and optical depth components are broken down into their across- and within-regime sub-components in rows 2 and 3, respectively.

SW cloud feedback is positive nearly everywhere equatorward of about 50° latitude and negative elsewhere, with large negative values centered around 60° in both hemispheres (Fig. 8a). Large positive feedbacks are present throughout the subtropical oceans and tropical land regions. This overall pattern emerges due to the superposition of a strong positive amount feedback (Fig. 8d) at low latitudes with maxima in the subtropics that falls to near-zero or weak negative values poleward of about 50° latitude, and a strong negative optical depth feedback (Fig. 8g) in the extratropics that peaks around 60° and that falls off or becomes weakly positive equatorward of about 40° latitude. Alternatively, one can describe the mean SW cloud feedback pattern as the superposition of a very spatially heterogeneous across-regime component (Fig. 8b) that closely matches the overall SW cloud feedback pattern, and a much more spatially homogeneous within-regime component (Fig. 8c) that is positive everywhere except at high latitudes.

As summarized in Sherwood et al. (2020), the positive low-latitude SW cloud amount feedbacks are consistent with a large body of work concluding that cloud cover should decrease with warming, including for tropical high clouds (Zelinka and Hartmann 2011; Bony et al. 2016), tropical marine low clouds (Myers and Norris 2016; Klein et al. 2017), and low clouds over land (Del Genio and Wolf 2000; Zhang and Klein 2013). Likewise, the latitudinally-varying response of cloud optical depth to warming is consistent with previous modeling studies, though observational analyses suggest a weaker negative extratropical feedback than produced in most models (Tselioudis et al. 1992; Eitzen et al. 2011; Gordon and Klein 2014; Terai et al. 2016; Myers et al. 2021).

The tendency for the SW cloud amount component (Fig. 8d) to be positive at low latitudes and small or negative at high latitudes is primarily established by the across-regime component (Fig. 8e), which shares this overall pattern. This means that, generally speaking, shifts from regimes with large cloud fraction to small cloud fraction occur at lower latitudes, particularly in the subtropics, and shifts from regimes with small cloud fraction to large cloud fraction occur at higher latitudes, with the overall radiative impact of these cloud amount changes being strongly muted ($0.05 \text{ W/m}^2/\text{K}$ on average; Fig. 8e). In contrast, the within-regime cloud amount feedback (Fig. 8f) is nearly uniformly positive across the globe, with substantial model agreement on the sign of the response (as indicated by the ubiquitous stippling). This indicates that, once controlling

for population shifts among regimes, the temperature mediated response of nearly all clouds globally is to decrease in areal coverage. This leads to a strong positive amount component from within-regime cloud property changes that is roughly equal to the full amount feedback. We will show below that this feedback component is uniformly positive even at the individual cloud regime level, not just when summing across cloud regimes. The local maxima in the amount feedback in the subtropics are regions where both the across- and within-components are positive. In these regions, both shifts towards regimes with smaller cloud fraction as well as decreases in cloud fraction within the regimes that are present reinforce one another. In contrast, the weak overall cloud amount feedback in the extratropics (Fig. 8d) arises because the negative contribution from shifts toward regimes with extensive cloud cover at the expense of regimes with less extensive cloud cover (Fig. 8e) counteracts the positive contribution from decreases in cloud fraction within the regimes that are present (Fig. 8f). Elucidation of which regimes are favored and disfavored with warming were discussed in Sect. 3.2 (Figs. 5 and 6) and their individual radiative contributions are discussed further below.

Consider now the SW cloud optical depth feedback and its sub-components (Fig. 8, row 3). In a similar way to the amount component, the across-regime optical depth sub-component (Fig. 8h) is small in the global mean but largely establishes the overall spatial structure of the optical depth feedback (Fig. 8g), while the within-regime sub-component (Fig. 8i) is much more uniformly negative and the dominant contributor to the global mean feedback. An exception is the Eastern Pacific stratocumulus regions, which exhibit robustly positive within-regime contributions to the optical depth feedback (Fig. 8i). Shifts from regimes with small optical depth to regimes with large optical depth occur at high latitudes, and these coincide with regions where the optical depth of clouds increases within the regimes already present, resulting in the very strong negative extratropical optical depth feedback (Fig. 8g–i). This is especially prominent over the Southern Ocean and the northern hemisphere midlatitude continents. In contrast, throughout much of the low-to-middle latitudes, the within- and across-regime sub-components oppose each other, resulting in weak overall optical depth feedback. For example in the North and South Pacific and southern Indian Oceans, shifts from thicker to thinner regimes make weak positive contributions to the optical depth feedback, but this is counteracted by the thickening of the clouds within regimes that are already present (Fig. 8g–i).

Returning to a question posed in the introduction, it is now clear that the negative SW cloud optical depth feedback over the Southern Ocean ($40\text{--}70^\circ \text{ S}$) receives contributions from both increased frequency of occurrence of thicker cloud types relative to thinner cloud types, as well as increases in

the albedo of clouds of a given morphology. Given that both components matter, we cannot focus solely on constraining changes in meteorology that determine cloud morphology or solely on constraining thermodynamic processes that affect cloud reflectivity within a given meteorological condition.

Let us briefly discuss the contributors to the across-regime and within-regime SW cloud feedbacks (Fig. 8, columns 2 and 3, respectively). The near-zero global mean across-regime feedback (Fig. 8b) results from the super-position of amount (Fig. 8e) and optical depth (Fig. 8h) sub-components that share very similar spatial structures—both are positive at low latitudes and negative at high latitudes, with nearly coincident zero-crossings at 45° latitude. This is to be expected because the regimes with large cloud fractions also have large optical depths (Table 2). Therefore, an increase in the RFO of cloudier/thicker regimes at the expense of less cloudy/thinner regimes will result in similar negative contributions to the amount and optical depth feedbacks (e.g., over the high latitudes), and vice versa. In contrast, the within-regime SW cloud feedback (Fig. 8c) results from a near-uniform positive amount sub-component (Fig. 8f) that is partially counteracted at most locations by a near-uniformly negative optical depth sub-component (Fig. 8i). The latter is large enough at high latitudes to dominate over the amount sub-component. What little spatial heterogeneity exists in the within-regime component belies the vast regions of the globe in Fig. 8f and Fig. 8i over which at least 8 out of 10 of the models agree on the sign of the feedback.

The results above indicate that much of the spatial structure of multi-model mean cloud feedback can be interpreted as due to changes in meteorology, which influences the relative amounts of the various cloud morphologies present, but which makes a small globally-averaged radiative impact. Excluding this component and focusing on the within-regime cloud changes, in contrast, highlights much more spatially uniform and systematic underlying cloud changes, whose radiative impact provides the dominant contribution to the globally averaged feedback.

To what extent is interpretation of the across- and within-regime feedback components complicated by the fact that regimes are defined by the cloud properties themselves rather than by exogenous fields characterizing relevant aspects of the meteorological environment (e.g., 500 hPa vertical velocity)? Consider a case where clouds of a given morphology at a given location thicken with warming. If this thickening is relatively small, one would expect this to be classified as a negative within-regime SW optical depth feedback. But if the thickening were sufficiently large, that location could be re-classified to a different, thicker cloud regime resulting in a negative *across-regime* SW optical depth feedback. Fundamentally, the same cloud property change occurred in both cases, but our analysis would ascribe different meanings to them, which is not desired.

It is worth recalling, however, that locations are assigned to regimes based on the combination of 3 cloud properties: albedo, cloud top pressure, and total cloud fraction, so it is not guaranteed that thickening would necessarily lead to reclassification to a thicker cloud regime if the cloud top pressure and total cloud fraction remain more similar to the original regime than to the thicker regime.

Nevertheless, if such a scenario were common, one would expect high pattern correlations between the within- and across-regime cloud feedback maps. Comparing the spatial patterns of the across-regime and within-regime feedbacks (Fig. 8, columns 2 and 3), it is clear that while there are some similarities, the patterns are largely distinct. Uncentered pattern correlations between the within-regime and across-regime SW amount feedback maps are 0.32 on average across models, with an across-model standard deviation of 0.21. For the optical depth component, the pattern correlation is 0.48 ± 0.16 . Hence while in some cases clouds of a given morphology may experience a large enough cloud property change that the resulting feedback is classified as across-regime rather than within-regime, this does not appear to be a common occurrence.

3.5 SW cloud feedback contributions from individual regimes

The SW cloud feedback and its components presented above are computed by summing across all 8 regimes. We can gain further insights into the processes contributing to these feedbacks by considering the contributions to the feedback from individual regimes. With the exception of Regime 1, the total SW cloud feedback is positive equatorward of about 50° in all regimes, then becomes strongly negative in the extratropics, with a negative peak at around 60° (Fig. 9a). Similar to the maps shown in Fig. 8, these features are closely mimicked by the across-regime component (Fig. 9b), whereas the within-regime component is uniformly positive in nearly all regimes and all latitudes except poleward of about 55° latitude (Fig. 9c).

The amount and optical depth sub-components of the across-regime feedback are shown in column 2 of Fig. 9. These panels are the SW cloud feedback counterpart to the actual change in RFO shown in Fig. 6b. Nearly everywhere, these two components act in the same direction, for reasons that were previously noted. For regimes characterized by thicker-than-average clouds and more extensive cloud cover (Regimes 2, 5, and 8), increased RFO in the extratropics (see Fig. 6b) causes negative SW cloud amount and optical depth feedback contributions, and decreased RFO at lower latitudes causes positive contributions (Fig. 9e, h). For regimes characterized by thinner-than-average clouds and less extensive cloud cover (Regimes 3 and 6), increased RFO at low latitudes causes *positive* SW cloud amount and

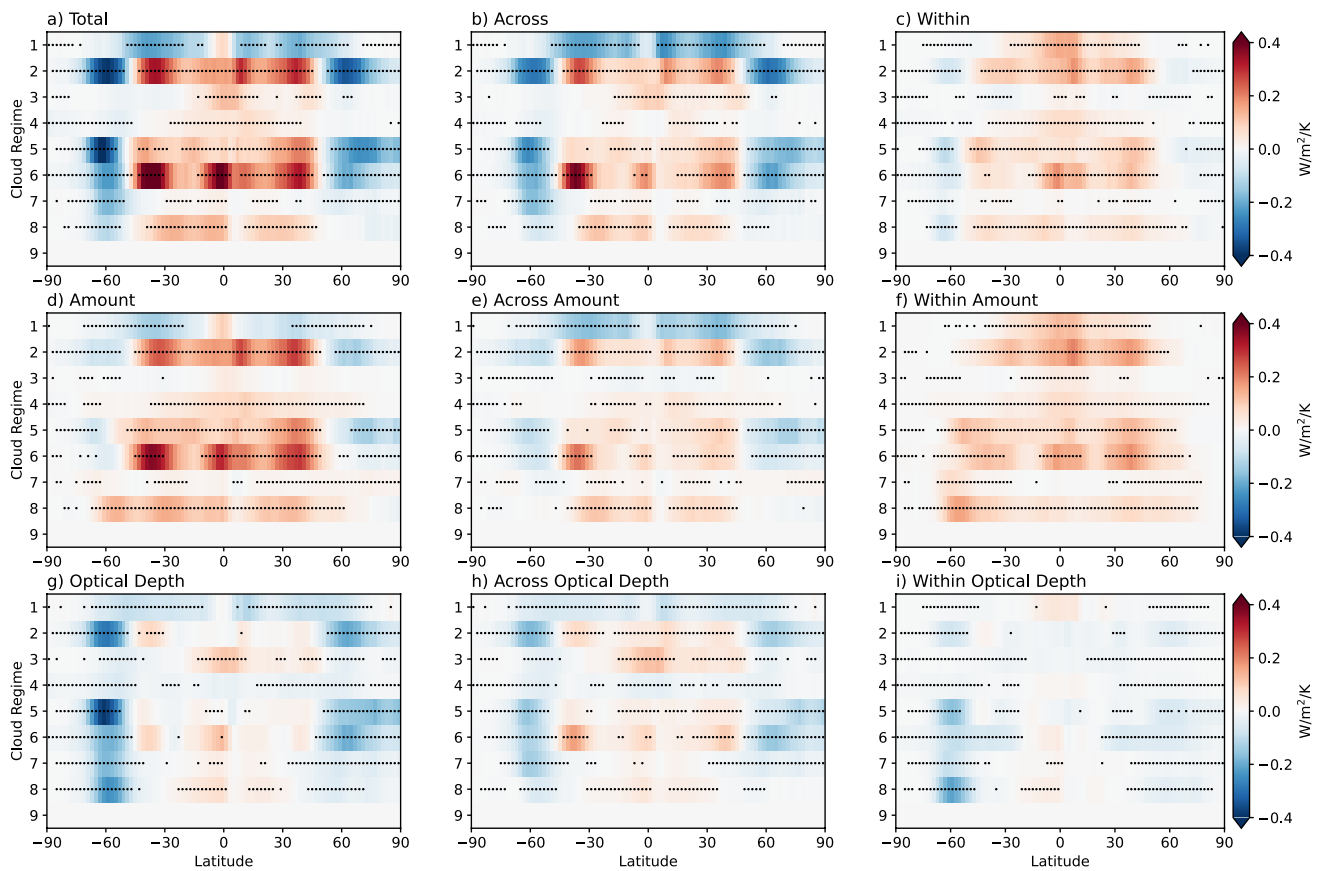


Fig. 9 As in Fig. 8, but showing the zonal mean contributions to the SW cloud feedback from each cloud regime. Stippling indicates locations where at least 8 out of 10 models agree on the sign of the change (not shown for clear-sky Regime 9)

optical depth feedback contributions, while decreased RFO in the extratropics causes *negative* contributions (Fig. 9e, h). The overall features of the across-regime component suggest a tendency for the cloud population to shift from cloudier and thicker regimes (Regimes 2, 5, 8) towards less-cloudy and thinner regimes (Regimes 3 and 6) at low latitudes, with the opposite response in the extratropics. This leads to an overall across-regime SW cloud feedback that is positive at low latitudes and negative at high latitudes (Fig. 9b). Below we will show that this basic pattern holds across all models.

One exception to this result is the behavior of Regime 1, for which the frequency of occurrence increases with warming at every latitude (see Fig. 6b). This causes uniformly negative amount and optical depth components because of the regime's relatively thick and extensive cloud cover. The global increase in the RFO of Regime 1 may be due to the overall upward shift of clouds with warming, such that some locations get reclassified from lower regimes into this high cloud regime.

Figure 9 column 3 shows the feedbacks from changes in cloud properties within the already-present regimes. As shown previously, not only are the global mean within-regime components uniform in sign across models, but

their geographic distributions are also nearly uniform in sign, with substantial inter-model agreement. In Fig. 9f and i we can see that this uniformity extends to regime space. That is, contributions to the SW cloud amount feedback are positive *within all individual regimes and at all latitudes*, particularly equatorward of about 60° (Fig. 9f). Similarly, contributions to the SW cloud optical depth feedback are negative *within all individual regimes poleward of about 40° latitude* (Fig. 9i). Hence, despite the wide diversity of cloud types and geographic distributions among the 8 regimes, they exhibit remarkably similar behavior in all regimes in response to warming (in the multi-model average): Clouds decrease in coverage at all latitudes and increase in albedo in the extratropics, causing positive amount and negative optical depth feedbacks, respectively.

3.6 SW cloud feedback contributions from individual models and between model generations

We now examine the zonal mean SW cloud feedback contributions in each of the ten individual models. The contributions to cloud feedback across all individual models agree

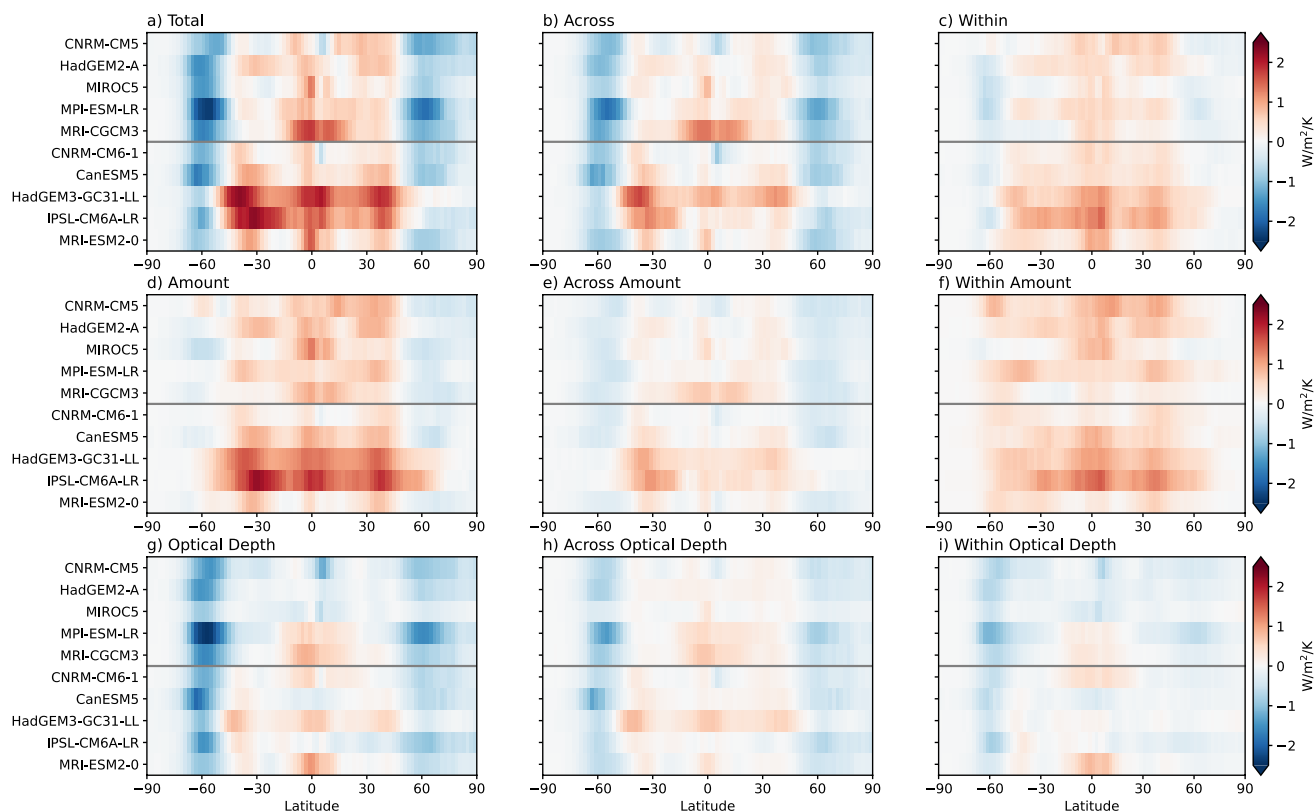


Fig. 10 As in Figure 8, but showing the zonal mean contributions to the SW cloud feedback from each model. Horizontal line separates CMIP5 models (above) from CMIP6 models (below)

qualitatively with the multi-model mean responses discussed previously, with inter-model differences primarily occurring in the relative magnitude of the responses as opposed to fundamental differences in geographic structure. For example, all models indicate a positive low-latitude feedback transitioning to a negative high-latitude feedback, with the former coming primarily from the amount component and the latter coming from the optical depth component. Previously we showed that the within-regime amount component is systematically positive across latitude and regime for the multi-model mean, and across all models for the global mean. We now see in Fig. 10f that it is systematically positive *across all models and latitudes* as well. Similarly, Fig. 10i confirms that the within-regime optical depth feedback is systematically negative at high latitudes *across all models*, with inter-model differences in sign at lower latitudes.

The extratropical SW cloud feedback has shifted towards stronger positive or weaker negative values between CMIP5 and CMIP6, which is a key driver of the increased climate sensitivity of these models (Zelinka et al. 2020). In the smaller subset of models considered here, we see this manifest in weaker negative feedbacks at high latitudes and stronger positive feedbacks at lower latitudes in the CMIP6 models (Fig. 11a). Consistent with Zelinka et al. (2020),

both the amount and optical depth feedbacks contribute to the shift, most dramatically in the extratropics (Fig. 11d, g). The latitude range experiencing positive amount and optical depth feedbacks has expanded poleward in CMIP6, most notably in HadGEM3-GGC31-LL and IPSL-CM6A-LR (Fig. 10a, d, g).

Whereas the within-regime component has shifted towards more positive values at all latitudes (Fig. 11c), this shift is confined mostly to the extratropics for the across-regime component (Fig. 11b). The shift of the within-regime component is primarily coming from a systematically stronger positive/weaker negative optical depth component (Fig. 11i), with a smaller contribution from a stronger positive amount component (Fig. 11f). The shift towards a weaker negative optical depth feedback in CMIP6 is consistent with a weaker cloud phase feedback owing to improved mean-state cloud phase in CMIP6 (Tan et al. 2016; McCoy et al. 2015). While this represents a shift towards better agreement with the broader body of evidence that this feedback is not strongly negative (Sherwood et al. 2020; Zelinka et al. 2022), it remains uncertain whether the improved mean-state necessarily means the latest models are better capturing all the physics needed for this feedback (Mülmenstädt et al. 2021).

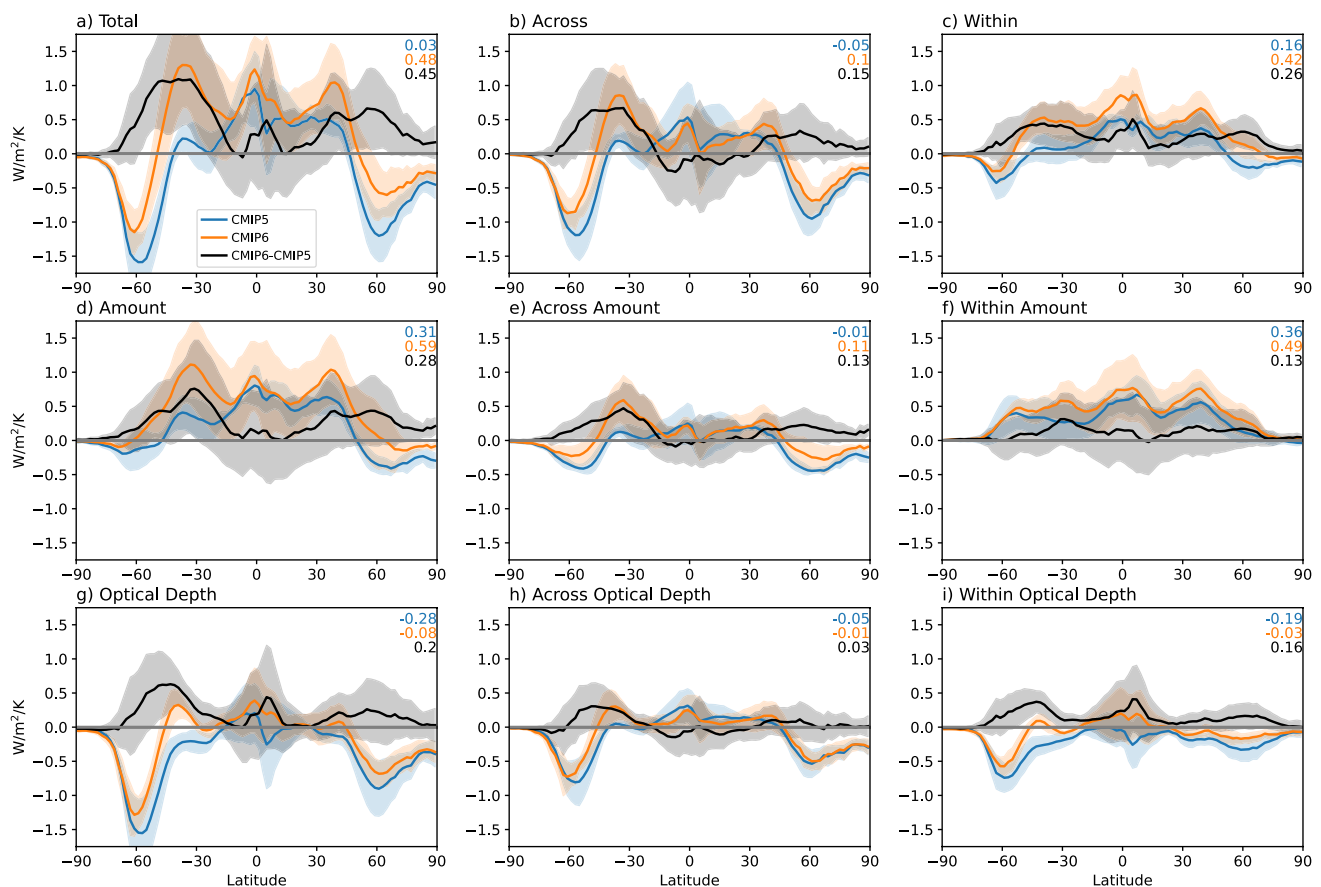


Fig. 11 Zonal mean contributions to the SW cloud feedback, averaged across CMIP5 (blue) and CMIP6 (orange) models. Solid lines represent the multi-model means and the shading spans the $\pm 1\sigma$ range across models. The difference between ensemble means is

shown in black, with the shading representing the combined uncertainty from summing the individual ensembles' 1σ ranges in quadrature. Global mean values are shown in the top right

The more-positive extratropical across-regime component in CMIP6 appears to receive roughly equal contributions from the amount and optical depth components (Fig. 11e, h). The notable large increase around 30–50 S is related to a much larger increase in the RFO of Regime 6—which has the thinnest and least extensive cloud coverage (not shown). In this same region, the cloudier/thicker Regime 5 decreases in CMIP6, whereas it increases in CMIP5 (not shown). At higher latitudes, the negative across-regime component has become weaker. This is because of a weaker increase in the RFO of cloudier/thicker Regimes 2 and 5 and a weaker decrease in the RFO of less-cloudy/thinner Regimes 6 and 7 in CMIP6 (not shown). Hence the shift away from thinner and less extensive cloud regimes towards thicker and more extensive cloud regimes at high latitudes is more muted in CMIP6, whereas the shift towards thinner / less extensive

cloud types at lower latitudes is a bit stronger in CMIP6. Both of these contribute to a more positive extratropical cloud feedback from across-regime shifts in CMIP6.

4 Conclusions and discussion

In this study we have brought together for the first time two diagnostic strategies that offer complementary information about the processes causing the cloud feedback. One, cloud radiative kernel analysis, allows for quantifying the cloud feedback arising from changes in cloud amount, altitude, and optical depth with warming. The other, cloud regime analysis, allows for determination of the feedback from changes in cloud properties within distinct cloud regimes separately from the feedback from changes in the relative occurrence frequencies of various

cloud regimes. Having first presented the mathematical basis for combining these techniques, we then presented novel insights about the cloud feedback that arise from applying the analysis to ten models from CMIP5 and CMIP6 simulating a uniform 4K increase in sea surface temperature. The analysis is performed for both longwave and shortwave cloud feedback but for brevity we focused herein on the shortwave cloud feedback results.

For any given model, both the within-regime and across-regime cloud feedback components can be substantial. However, their roles are rather different: In the global average, the across-regime components tend to exhibit substantial inter-model spread but a negligible ensemble-mean contribution. Their geographic structures, however, largely determine the spatial pattern of the total SW cloud feedback. These patterns reflect the fact that thinner, less extensive cloud types increase at the expense of thicker, more extensive cloud types at low latitudes, with the opposite response at high latitudes, leading to an overall positive across-regime component at low latitudes and negative across-regime component at high latitudes.

In contrast, the global mean within-regime components tend to be of uniform sign across models (systematically positive for cloud amount and nearly systematically negative but of weaker magnitude for cloud optical depth), such that they are the primary contributor to the positive ensemble-mean SW cloud feedback. Their spatial patterns are very homogeneous, with near-uniform positive contributions from cloud amount decreases and near-uniform weaker negative contributions from cloud albedo increases.

Results are highly consistent when we perform the same analysis but with the models' clouds matched to the 11 MODIS cloud regimes of Cho et al. (2021) rather than the 8 ISCCP cloud regimes of Tselioudis et al. (2021), as shown in the Supplementary Information. One quantitative difference is that the ensemble mean across-regime amount component increases in strength slightly relative to those shown here (compare Fig. 8e with SI Fig. 3e), and the within-regime amount component decreases in strength slightly (compare Fig. 8f with SI Fig. 3f). This is unsurprising, as the likelihood of a location being reclassified to a different cloud regime in a warmed climate increases as the number of regimes increases, owing to the necessarily more subtle inter-regime differences in cloud properties when more regimes are present. It remains the case, however, that the ensemble mean across-regime feedback is near zero and the within-regime feedback is by far the dominant contributor to the overall feedback (compare Fig. 7 with SI Fig. 2). This indicates that our overall qualitative results are insensitive to the choice of observational cloud regimes to which the model fields are assigned.

Substantial model-to-model variations in the across-regime cloud feedback component are likely tied to

variations in how large-scale meteorology—and the cloud regimes that it (dis)favors – changes with warming. However, these changes are not systematic across models, so the multi-model mean across-regime feedback is near zero. In contrast, very consistent feedbacks from temperature-mediated decreases in cloud coverage and increases in cloud optical depth are revealed once the obfuscating effects of changing large-scale meteorology are removed. The latter result is true even when considering individual cloud regimes, which exhibit systematic changes at all latitudes.

The negative optical depth feedback over the Southern Ocean receives contributions from both the increased frequency of occurrence of thicker cloud types relative to thinner cloud types, as well as increases in the albedo of clouds of a given morphology. This means that changes in meteorology that determine cloud morphology as well as thermodynamic processes that affect cloud reflectivity within a given meteorological condition are important.

CMIP6 models exhibit weaker negative feedbacks at high latitudes and stronger positive feedbacks at lower latitudes than their predecessors in CMIP5, consistent with previous work (Zelinka et al. 2020; Flynn and Mauritsen 2020). Both cloud amount and optical depth feedbacks contribute to this shift, most dramatically in the extratropics. Within regimes, the decrease of cloud amount is greater in CMIP6, while the increase in cloud albedo is weaker in CMIP6, possibly related to increased mean-state supercooled liquid fractions that weaken the phase feedback. Additionally, the increased frequency of thicker/cloudier regimes at high latitudes is less dramatic in CMIP6, while the shift towards thinner/less-cloudy regimes at lower latitudes is more dramatic, both of which contribute to a more positive across-regime extratropical feedback in CMIP6.

To the extent that internal climate variability and long-term greenhouse warming lead to distinct changes in large-scale circulation, whereas the response of cloud properties to warming within meteorological regimes is timescale-invariant, future work should investigate whether across-timescale correspondence of cloud feedback improves if considering only the within-regime component. If so, this could provide an effective strategy for constraining a portion of cloud feedback, especially in regions where changes in large-scale meteorology or model biases in control-climate meteorology (Kelleher and Grise 2022) may obscure the otherwise close relationship between temperature-mediated changes in cloud properties of a given morphology across time scales.

Supplementary Information The online version contains supplementary material available at <https://doi.org/10.1007/s00382-022-06488-7>.

Acknowledgements We acknowledge the World Climate Research Programme, which, through its Working Group on Coupled Modelling, coordinated and promoted CMIP. We thank the climate modeling

groups for producing and making available their model output, the Earth System Grid Federation (ESGF) for archiving the data and providing access, and the multiple funding agencies who support CMIP and ESGF. We thank two anonymous reviewers for helpful suggestions for improvements to the manuscript, Daeho Jin for guidance with normalization, and Yoko Tsushima, Karl Taylor, and Steve Klein for useful discussions.

Author contributions All authors contributed to the study conception and design. Data analysis was performed by MDZ. The first draft of the manuscript was written by MDZ and all authors commented on subsequent versions of the manuscript. All authors read and approved the final manuscript.

Funding MDZ and IT were supported by NASA grant 80NSSC-18K1599. MDZ's work was additionally supported by the U.S. Department of Energy (DOE) Regional and Global Model Analysis program area and was performed under the auspices of the DOE by Lawrence Livermore National Laboratory under Contract DE-AC52-07NA27344. LO and GT were supported by the NASA MEaSUREs program.

Availability of data and materials ISCCP HGG weather states are available at <https://isccp.giss.nasa.gov/wstates/hggws.html>. Cloud radiative kernels are available at <https://doi.org/10.5281/zenodo.5514137> (Zelinka 2021).

Code availability Python code to perform all calculations and produce all figures and tables in this manuscript are available at <https://doi.org/10.5281/zenodo.7062949>.

Declarations

Conflict of interest The authors have no relevant financial or non-financial interests to disclose.

Ethics approval Not applicable

Consent to participate: Not applicable

Consent for publication Not applicable

References

- Barnes EA, Polvani L (2013) Response of the midlatitude jets, and of their variability, to increased greenhouse gases in the CMIP5 models. *J Clim* 26(18):7117–7135. <https://doi.org/10.1175/jcli-d-12-00536.1>
- Bodas-Salcedo A, Williams KD, Field PR, Lock AP (2012) The surface downwelling solar radiation surplus over the southern ocean in the met office model: the role of midlatitude cyclone clouds. *J Clim* 25(21):7467–7486. <https://doi.org/10.1175/jcli-d-11-00702.1>
- Bodas-Salcedo A, Williams KD, Ringer MA, Beau I, Cole JNS, Dufresne JL, Koshiro T, Stevens B, Wang Z, Yokohata T (2014) Origins of the solar radiation biases over the Southern Ocean in CFMIP2 models. *J Clim* 27(1):41–56. <https://doi.org/10.1175/JCLI-D-13-00169.1>. <https://journals.ametsoc.org/view/journals/clim/27/1/jcli-d-13-00169.1.xml>
- Bony S, Dufresne JL (2005) Marine boundary layer clouds at the heart of tropical cloud feedback uncertainties in climate models. *Geophys Res Lett*. <https://doi.org/10.1029/2005GL023851>
- Bony S, Lau KM, Sud YC (1997) Sea surface temperature and large-scale circulation influences on tropical greenhouse effect and cloud radiative forcing. *J Clim* 10:2055–2077. [https://doi.org/10.1175/1520-0442\(1997\)0102.0.CO;2](https://doi.org/10.1175/1520-0442(1997)0102.0.CO;2)
- Bony S, Dufresne JL, Treut HL, Morcrette JJ, Senior C (2004) On dynamic and thermodynamic components of cloud changes. *Clim Dyn* 22:71–86. <https://doi.org/10.1007/s00382-003-0369-6>
- Bony S, Stevens B, Coppin D, Becker T, Reed KA, Voigt A, Medeiros B (2016) Thermodynamic control of anvil cloud amount. *Proc Natl Acad Sci*. <https://doi.org/10.1073/pnas.1601472113>
- Boucher O, Servonnat J, Albright AL, Aumont O, Balkanski Y, Bastrikov V, Bekki S, Bonnet R, Bony S, Bopp L, Braconnot P, Brockmann P, Cadule P, Caubel A, Cheruy F, Codron F, Cozic A, Cugnet D, D'Andrea F, Davini P, Lavergne Cd, Denvil S, Deshayes J, Devilliers M, Ducharne A, Dufresne JL, Dupont E, Éthé C, Fairhead L, Falletti L, Flavoni S, Foujols MA, Gardoll S, Gastineau G, Ghattas J, Grandpeix JY, Guenet B, Guez L E, Guilyardi E, Guimberteau M, Hauglustaine D, Hourdin F, Idelkadi A, Joussaume S, Kageyama M, Khodri M, Krinner G, Lebas N, Levavasseur G, Lévy C, Li L, Lott F, Lurton T, Luysaert S, Madec G, Madeleine JB, Maignan F, Marchand M, Marti O, Mellul L, Meurdesoif Y, Mignot J, Musat I, Otlé C, Peylin P, Planton Y, Polcher J, Rio C, Rochetin N, Rousset C, Sepulchre P, Sima A, Swingedouw D, Thiéblemont R, Traore AK, Vancoppenolle M, Vial J, Vialard J, Viovy N, Vuichard N (2020) Presentation and evaluation of the IPSL-CM6A-LR climate model. *J Adv Model Earth Syst* 12(7):e2019MS002,010. <https://doi.org/10.1029/2019MS002010>. <https://agupubs.onlinelibrary.wiley.com/doi/abs/10.1029/2019MS002010>, <https://agupubs.onlinelibrary.wiley.com/doi/pdf/10.1029/2019MS002010>
- Cho N, Tan J, Oreopoulos L (2021) Classifying planetary cloudiness with an updated set of MODIS cloud regimes. *J Appl Meteorol Climatol* 60(7):981–997. <https://doi.org/10.1175/JAMC-D-20-0247.1>. <https://journals.ametsoc.org/view/journals/apme/aop/JAMC-D-20-0247.1/JAMC-D-20-0247.1.xml>
- Collins WJ, Bellouin N, Doutriaux-Boucher M, Gedney N, Hinton PHT, Hughes J, Jones CD, Joshi M, Liddicoat S, Martin G, O'Connor F, Rae J, Senior C, Sitch S, Totterdell I, Wiltshire A, Woodward S (2011) Development and evaluation of an earth-system model—HadGEM2. *Geosci Model Dev Discuss* 4:997–1062
- Del Genio AD, Wolf AB (2000) The temperature dependence of the liquid water path of low clouds in the southern Great Plains. *J Clim* 13(19):3465–3486. [https://doi.org/10.1175/1520-0442\(2000\)013<3465:ttdotl>2.0.co;2](https://doi.org/10.1175/1520-0442(2000)013<3465:ttdotl>2.0.co;2)
- Eitzen ZA, Xu KM, Wong T (2011) An estimate of low-cloud feedbacks from variations of cloud radiative and physical properties with sea surface temperature on interannual time scales. *J Clim* 24(4):1106–1121. <https://doi.org/10.1175/2010jcli3670.1>
- Eyring V, Bony S, Meehl GA, Senior CA, Stevens B, Stouffer RJ, Taylor KE (2016) Overview of the Coupled Model Intercomparison Project Phase 6 (CMIP6) experimental design and organization. *Geosci Model Dev* 9(5):1937–1958. <https://doi.org/10.5194/gmd-9-1937-2016>
- Flynn CM, Mauritsen T (2020) On the climate sensitivity and historical warming evolution in recent coupled model ensembles. *Atmos Chem Phys* 20(13):7829–7842. <https://doi.org/10.5194/acp-20-7829-2020>. <https://acp.copernicus.org/articles/20/7829/2020/>
- Gordon ND, Klein SA (2014) Low-cloud optical depth feedback in climate models. *J Geophys Res Atmos* 119(10):6052–6065. <https://doi.org/10.1002/2013jd021052>
- Gordon ND, Norris JR (2010) Cluster analysis of midlatitude oceanic cloud regimes: mean properties and temperature sensitivity. *Atmos Chem Phys* 10(13):6435–6459. <https://doi.org/10.5194/acp-10-6435-2010>

- Gordon ND, Norris JR, Weaver CP, Klein SA (2005) Cluster analysis of cloud regimes and characteristic dynamics of midlatitude synoptic systems in observations and a model. *J Geophys Res Atmos*. <https://doi.org/10.1029/2004jd005027>
- Hartmann DL, Larson K (2002) An important constraint on tropical cloud-climate feedback. *Geophys Res Lett*. <https://doi.org/10.1029/2002GL015835>
- Jakob C, Tselioudis G (2003) Objective identification of cloud regimes in the Tropical Western Pacific. *Geophys Res Lett* 30(21). <https://doi.org/10.1029/2003GL018367>. <https://onlinelibrary.wiley.com/doi/abs/10.1029/2003GL018367>
- Jin D, Oreopoulos L, Lee D (2017a) Regime-based evaluation of cloudiness in CMIP5 models. *Clim Dyn* 48(1):89–112. <https://doi.org/10.1007/s00382-016-3064-0>
- Jin D, Oreopoulos L, Lee D (2017b) Simplified ISCCP cloud regimes for evaluating cloudiness in CMIP5 models. *Clim Dyn* 48(1):113–130. <https://doi.org/10.1007/s00382-016-3107-6>
- Kelleher MK, Grise KM (2022) Varied midlatitude shortwave cloud radiative responses to Southern Hemisphere circulation shifts. *Atmos Sci Lett* 23(1):e1068. <https://doi.org/10.1002/asl.1068>. <https://onlinelibrary.wiley.com/doi/abs/10.1002/asl.1068>
- Klein SA, Jakob C (1999) Validation and sensitivities of frontal clouds simulated by the ECMWF model. *Mon Weath Rev* 127:2514–2531. [https://doi.org/10.1175/1520-0493\(1999\)127.0.CO;2](https://doi.org/10.1175/1520-0493(1999)127.0.CO;2)
- Klein SA, Hall A, Norris JR, Pincus R (2017) Low-cloud feedbacks from cloud-controlling factors: a review. *Surv Geophys*. <https://doi.org/10.1007/s10712-017-9433-3>
- McCoy DT, Hartmann DL, Zelinka MD, Ceppi P, Grosvenor DP (2015) Mixed-phase cloud physics and Southern Ocean cloud feedback in climate models. *J Geophys Res Atmos* 120(18):9539–9554. <https://doi.org/10.1002/2015jd023603>
- McCoy DT, Field PR, Elsaesser GS, Bodas-Salcedo A, Kahn BH, Zelinka MD, Kodama C, Mauritsen T, Vanniere B, Roberts M, Vidale PL, Saint-Martin D, Voltaire A, Haarsma R, Hill A, Shipway B, Wilkinson J (2019) Cloud feedbacks in extratropical cyclones: insight from long-term satellite data and high-resolution global simulations. *Atmos Chem Phys* 19(2):1147–1172. <https://doi.org/10.5194/acp-19-1147-2019>
- McCoy DT, Field P, Bodas-Salcedo A, Elsaesser GS, Zelinka MD (2020) A regime-oriented approach to observationally constraining extratropical shortwave cloud feedbacks. *J Clim* 33(23):9967–9983. <https://doi.org/10.1175/JCLI-D-19-0987.1>. <https://journals.ametsoc.org/view/journals/clim/33/23/jcliD190987.xml>
- Mülmenstädt J, Salzmann M, Kay JE, Zelinka MD, Ma PL, Nam C, Kretzschmar J, Hörnig S, Quaas J (2021) An underestimated negative cloud feedback from cloud lifetime changes. *Nat Clim Change* 11(6):508–513. <https://doi.org/10.1038/s41558-021-01038-1>. <https://www.nature.com/articles/s41558-021-01038-1>
- Myers TA, Norris JR (2016) Reducing the uncertainty in subtropical cloud feedback. *Geophys Res Lett* 43(5):2144–2148. <https://doi.org/10.1002/2015gl067416>
- Myers TA, Scott RC, Zelinka MD, Klein SA, Norris JR, Caldwell PM (2021) Observational constraints on low cloud feedback reduce uncertainty of climate sensitivity. *Nat Clim Change* 11(6):501–507. <https://doi.org/10.1038/s41558-021-01039-0>. <https://www.nature.com/articles/s41558-021-01039-0>
- Norris JR, Iacobellis SF (2005) North Pacific cloud feedbacks inferred from synoptic-scale dynamic and thermodynamic relationships. *J Clim* 18(22):4862–4878. <https://doi.org/10.1175/jcli3558.1>
- Oreopoulos L, Rossow WB (2011) The cloud radiative effects of International Satellite Cloud Climatology Project weather states. *J Geophys Res Atmos*. <https://doi.org/10.1029/2010jd015472>
- Rossow W, Walker A, Beusichel D, Roiter M (1996) International Satellite Cloud Climatology Project (ISCCP) Documentation of New Cloud Datasets. WMO/TD-No 737, World Meteorological Organization, 115 pp
- Sherwood SC, Webb MJ, Annan JD, Armour KC, Forster PM, Hargreaves JC, Hegerl G, Klein SA, Marvel KD, Rohling EJ, Watanabe M, Andrews T, Braconnot P, Bretherton CS, Foster GL, Hausfather Z, Heydt ASvd, Knutti R, Mauritsen T, Norris JR, Proistosescu C, Rugenstein M, Schmidt GA, Tokarska KB, Zelinka MD (2020) An assessment of earth's climate sensitivity using multiple lines of evidence. *Rev Geophys* 58(4):e2019RG000,678. <https://doi.org/10.1029/2019RG000678>. <https://agupubs.onlinelibrary.wiley.com/doi/abs/10.1029/2019RG000678>
- Soden BJ, Broccoli AJ, Hemler RS (2004) On the use of cloud forcing to estimate cloud feedback. *J Clim* 17:3661–3665. [https://doi.org/10.1175/1520-0442\(2004\)017.0.CO;2](https://doi.org/10.1175/1520-0442(2004)017.0.CO;2)
- Soden BJ, Held IM, Colman R, Shell KM, Kiehl JT, Shields CA (2008) Quantifying climate feedbacks using radiative kernels. *J Clim* 21:3504–3520. <https://doi.org/10.1175/2007JCLI2110.1>
- Stevens B, Giorgetta M, Esch M, Mauritsen T, Crueger T, Rast S, Salzmann M, Schmidt H, Bader J, Block K, Brokopf R, Fast I, Kinne S, Kornbluh L, Lohmann U, Pincus R, Reichler T, Roeckner E (2013) Atmospheric component of the MPI-M Earth System Model: ECHAM6. *J Adv Model Earth Syst* 5(2):146–172. <https://doi.org/10.1002/jame.20015>
- Swart NC, Cole JNS, Kharin VV, Lazare M, Scinocca JF, Gillett NP, Anstey J, Arora V, Christian JR, Hanna S, Jiao Y, Lee WG, Majaess F, Saenko OA, Seiler C, Seinen C, Shao A, Sigmond M, Solheim L, von Salzen K, Yang D, Winter B (2019) The Canadian earth system model version 5 (CanESM5.0.3). *Geosci Model Dev* 12(11):4823–4873. <https://doi.org/10.5194/gmd-12-4823-2019>. <https://gmd.copernicus.org/articles/12/4823/2019/>
- Tan I, Storelvmo T, Zelinka MD (2016) Observational constraints on mixed-phase clouds imply higher climate sensitivity. *Science* 352(6282):224–227. <https://doi.org/10.1126/science.aad5300>
- Taylor KE, Stouffer RJ, Meehl GA (2012) An overview of CMIP5 and the experiment design. *Bull Amer Meteor Soc* 93(4):485–498. <https://doi.org/10.1175/BAMS-D-11-00094.1>
- Terai CR, Klein SA, Zelinka MD (2016) Constraining the low-cloud optical depth feedback at middle and high latitudes using satellite observations. *J Geophys Res Atmos* 121(16):9696–9716. <https://doi.org/10.1002/2016jd025233>
- Thompson DWJ, Bony S, Li Y (2017) Thermodynamic constraint on the depth of the global tropospheric circulation. *Proc Natl Acad Sci*. <https://doi.org/10.1073/pnas.1620493114>
- Tselioudis G, Rossow WB (2006) Climate feedback implied by observed radiation and precipitation changes with midlatitude storm strength and frequency. *Geophys Res Lett*. <https://doi.org/10.1029/2005gl024513>
- Tselioudis G, Rossow WB, Rind D (1992) Global patterns of cloud optical thickness variation with temperature. *J Clim* 5:1484–1495. [https://doi.org/10.1175/1520-0442\(1992\)0052.0.CO;2](https://doi.org/10.1175/1520-0442(1992)0052.0.CO;2)
- Tselioudis G, Rossow WB, Jakob C, Remillard J, Trof D, Zhang Y (2021) Evaluation of clouds, radiation, and precipitation in CMIP6 models using global weather states derived from ISCCP-H cloud property data. *J Clim* 34(17):7311–7324. <https://doi.org/10.1175/JCLI-D-21-0076.1>. <https://journals.ametsoc.org/view/journals/clim/aop/JCLI-D-21-0076.1/JCLI-D-21-0076.1.xml>
- Tsushima Y, Ringer MA, Webb MJ, Williams KD (2013) Quantitative evaluation of the seasonal variations in climate model cloud regimes. *Clim Dyn* 41(9):2679–2696. <https://doi.org/10.1007/s00382-012-1609-4>
- Tsushima Y, Ringer MA, Koshiro T, Kawai H, Roehrig R, Cole J, Watanabe M, Yokohata T, Bodas-Salcedo A, Williams KD, Webb MJ (2016) Robustness, uncertainties, and emergent constraints in the radiative responses of stratocumulus cloud regimes to future warming. *Clim Dyn* 46(9):3025–3039. <https://doi.org/10.1007/s00382-015-2750-7>

- Voltaire A, Saint-Martin D, S n si S, Decharme B, Alias A, Chevalier M, Colin J, Gu r my JF, Michou M, Moine MP, Nabat P, Roehrig R, M lia DSy, S f rian R, Valcke S, Beau I, Belamari S, Berthet S, Cassou C, Cattiaux J, Deshayes J, Douville H, Eth  C, Franchist guy L, Geoffroy O, L vy C, Madec G, Meurdesoif Y, Msadek R, Ribes A, Sanchez-Gomez E, Terray L, Waldman R (2019) Evaluation of CMIP6 DECK experiments with CNRM-CM6-1. *J Adv Model Earth Syst* 11(7):2177–2213. <https://doi.org/10.1029/2019MS001683>. <https://agupubs.onlinelibrary.wiley.com/doi/abs/10.1029/2019MS001683>, _eprint: <https://agupubs.onlinelibrary.wiley.com/doi/pdf/10.1029/2019MS001683>
- Watanabe M, Suzuki T, Oishi R, Komuro Y, Watanabe S, Emori S, Takemura T, Chikira M, Ogura T, Sekiguchi M, Takata K, Yamazaki D, Yokohata T, Nozawa T, Hasumi H, Tatebe H, Kimoto M (2010) Improved climate simulation by MIROC5: mean states, variability, and climate sensitivity. *J Clim* 23(23):6312–6335. <https://doi.org/10.1175/2010JCLI3679.1>. <https://journals.ametsoc.org/view/journals/clim/23/23/2010jcli3679.1.xml>
- Webb M, Senior C, Bony S, Morcrette JJ (2001) Combining ERBE and ISCCP data to assess clouds in the Hadley Centre, ECMWF and LMD atmospheric climate models. *Clim Dyn* 17:905–922. <https://doi.org/10.1007/s003820100157>
- Williams K, Tselioudis G (2007) GCM intercomparison of global cloud regimes: present-day evaluation and climate change response. *Clim Dyn* 29:231–250. <https://doi.org/10.1007/s00382-007-0232-2>
- Williams K, Webb M (2009) A quantitative performance assessment of cloud regimes in climate models. *Clim Dyn* 33:141–157. <https://doi.org/10.1007/s00382-008-0443-1>
- Williams KD, Copsey D, Blockley EW, Bodas-Salcedo A, Calvert D, Comer R, Davis P, Graham T, Hewitt HT, Hill R, Hyder P, Ineson S, Johns TC, Keen AB, Lee RW, Megann A, Milton SF, Rae JGL, Roberts MJ, Scaife AA, Schiemann R, Storky D, Thorpe L, Watterson IG, Walters DN, West A, Wood RA, Woollings T, Xavier PK (2018) The met office global coupled model 3.0 and 3.1 (GC3.0 and GC3.1) configurations. *J Adv Model Earth Syst* 10(2):357–380. <https://doi.org/10.1002/2017MS001115>. <https://agupubs.onlinelibrary.wiley.com/doi/abs/10.1002/2017MS001115>, _eprint: <https://agupubs.onlinelibrary.wiley.com/doi/pdf/10.1002/2017MS001115>
- Yin JH (2005) A consistent poleward shift of the storm tracks in simulations of 21st century climate. *Geophys Res Lett*. <https://doi.org/10.1029/2005GL023684>
- Yukimoto S, Adachi Y, Hosaka M, Sakami T, Yoshimura H, Hirabara M, Tanaka TY, Shindo E, Tsujino H, Deushi M, Mizuta R, Yabu S, Obata A, Nakano H, Koshiro T, Ose T, Kitoh A (2012) A new global climate model of the meteorological research institute: MRI-CGCM3—model description and basic performance. *J Meteorol Soc Jpn Ser II* 90A:23–64. <https://doi.org/10.2151/jmsj.2012-A02>
- Yukimoto S, Kawai H, Koshiro T, Oshima N, Yoshida K, Urakawa S, Tsujino H, Deushi M, Tanaka T, Hosaka M, Yabu S, Yoshimura H, Shindo E, Mizuta R, Obata A, Adachi Y, Ishii M (2019) The meteorological research institute earth system model version 2.0, MRI-ESM2.0: description and basic evaluation of the physical component. *J Meteorol Soc Jpn Ser II* 97(5):931–965. <https://doi.org/10.2151/jmsj.2019-051>
- Zelinka M (2021) mzelinka/cloud-radiative-kernels: Sep 17, 2021 Release. <https://doi.org/10.5281/zenodo.5514137>. <https://zenodo.org/record/5514137>
- Zelinka MD, Hartmann DL (2011) The observed sensitivity of high clouds to mean surface temperature anomalies in the tropics. *J Geophys Res Atmos*. <https://doi.org/10.1029/2011JD016459>
- Zelinka MD, Klein SA, Hartmann DL (2012a) Computing and partitioning cloud feedbacks using cloud property histograms. Part I: cloud radiative kernels. *J Clim* 25(11):3715–3735. <https://doi.org/10.1175/jcli-d-11-00248.1>
- Zelinka MD, Klein SA, Hartmann DL (2012b) Computing and partitioning cloud feedbacks using cloud property histograms. Part II: attribution to changes in cloud amount, altitude, and optical depth. *J Clim* 25(11):3736–3754. <https://doi.org/10.1175/JCLI-D-11-00249.1>
- Zelinka MD, Klein SA, Taylor KE, Andrews T, Webb MJ, Gregory JM, Forster PM (2013) Contributions of different cloud types to feedbacks and rapid adjustments in CMIP5. *J Clim* 26(14):5007–5027. <https://doi.org/10.1175/jcli-d-12-00555.1>
- Zelinka MD, Zhou C, Klein SA (2016) Insights from a refined decomposition of cloud feedbacks. *Geophys Res Lett* 43(17):9259–9269. <https://doi.org/10.1002/2016gl069917>
- Zelinka MD, Myers TA, McCoy DT, Po-Chedley S, Caldwell PM, Ceppi P, Klein SA, Taylor KE (2020) Causes of higher climate sensitivity in CMIP6 models. *Geophys Res Lett* 47(1):e2019GL085782. <https://doi.org/10.1029/2019GL085782>. <https://agupubs.onlinelibrary.wiley.com/doi/abs/10.1029/2019GL085782>
- Zelinka MD, Klein SA, Qin Y, Myers TA (2022) Evaluating climate models' cloud feedbacks against expert judgment. *J Geophys Res Atmos* 127(2):e2021JD035198. <https://doi.org/10.1029/2021JD035198>. <https://onlinelibrary.wiley.com/doi/abs/10.1029/2021JD035198>, _eprint: <https://onlinelibrary.wiley.com/doi/pdf/10.1029/2021JD035198>
- Zhang Y, Klein SA (2013) Factors controlling the vertical extent of fair-weather shallow cumulus clouds over land: investigation of diurnal-cycle observations collected at the ARM southern great plains site. *J Atmos Sci* 70(4):1297–1315. <https://doi.org/10.1175/JAS-D-12-0131.1>. <https://journals.ametsoc.org/view/journals/atsc/70/4/jas-d-12-0131.1.xml>

Publisher's Note Springer Nature remains neutral with regard to jurisdictional claims in published maps and institutional affiliations.

Springer Nature or its licensor holds exclusive rights to this article under a publishing agreement with the author(s) or other rightsholder(s); author self-archiving of the accepted manuscript version of this article is solely governed by the terms of such publishing agreement and applicable law.